Inflammation associated altered nucleic acid levels and localization

A Thesis

submitted to

Indian Institute of Science Education and Research Pune in partial fulfilment of the requirements for the BS-MS Dual Degree Programme

by

Aishwarya Juneja

Indian Institute of Science Education and Research Pune

Dr. Homi Bhabha Road,

Pashan, Pune 411008, INDIA.

Date: 10th April, 2023

Under the guidance of

Supervisor: Dr. Shovamayee Maharana, IISc

Expert: Dr. Kundan Sengupta, IISER Pune

Co-supervisor: Dr. Nikhil Gandasi, IISc

From June 2022 to Apr 2023

INDIAN INSTITUTE OF SCIENCE EDUCATION AND RESEARCH PUNE

Certificate

This is to certify that this dissertation entitled **"Inflammation associated altered nucleic acid levels and localization"** towards the partial fulfilment of the BS-MS dual degree programme at the Indian Institute of Science Education and Research, Pune represents work carried out by Aishwarya Juneja at Indian Institute of Science (IISc) under the supervision of Dr. Shovamayee Mahara, Professor, Department of Microbiology and Cell Biology, during the academic year 2022-2023.

Name of your Guide

Dr. Shovamayee Maharana

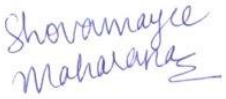

TAC members:

Expert: Dr. Kundan Sengupta

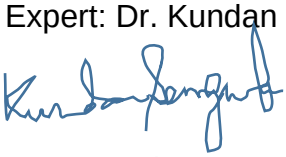

Co-supervisor: Dr. Nikhil Gandasi

This thesis is dedicated to my younger sister, Riddhi, who patiently awaits my return.

Declaration

I hereby declare that the matter embodied in the report entitled "**Inflammation associated altered nucleic acid levels and localization"** are the results of the work carried out by me at the Department of Microbiology and Cell Biology, Indian Institute of Science, Bangalore, under the supervision of Dr. Shovamayee Maharana for my Master's project at Indian Institute of Science, Education, and Research, Pune. The same has not been submitted elsewhere for any other degree.

Name: Aishwarya Juneja

Date: 10-04-23

Table of Contents

List of Tables

List of Figures

List of Abbreviations

ADAR1 - Adenosine deaminase 1
AIM2- Absent in Melanoma 2
AMP - Adenosine monophosphate
AP-2 - Adaptor Protein 2
ATP - Adenosine triphosphate
cGAMP - cyclic GMP-AMP
cGAS - cyclic GMP-AMP synthase
CLR - C- type lectin receptors
CpG - Cytosine-phosphate-guanine
DAMP - Danger-associated molecular patterns
DNA - Deoxyribonucleic acid
dsDNA - double stranded DNA
dsRNA - double stranded RNA
eIF2α - Eukaryotic Initiation Factor 2
ER - Endoplasmic Reticulum
G3BP1 - GTPase-activating protein-binding protein 1
GMP - Guanosine monophosphate
IFNβ - Interferon beta
IL1-β - Interleukin 1 beta
IL-6 - Interleukin-6
IRF - Interferon regulatory factor
ISG - Interferon-stimulated genes
JAK- Janus Kinase signal transducer and activator of transcription proteins
LRR - Leucine Rich Repeat
MDA-5 - Melanoma differentiation antigen 5
MYD 88 - Myeloid differentiation primary response 88
NFKB - Nuclear Factor Kappa- B
NLR - Nucleotide oligomerization domain like receptors
NOD - Nucleotide oligomerization domain
OAS - Oligoadenylate synthase
PAMP - Pathogen-associated molecular patterns
PEI - Polycation polyethylenimine

Poly I:C - Polyinosinic polycytidylic acid (Poly(I)・Poly(C))

PKR - RNA-dependent Protein Kinase

PRR - Pattern recognition receptors

RBP - RNA-binding protein

RIG-I - Retinoic acid-inducible gene I

RNA - Ribonucleic acid

RNase L – Ribonuclease L

RLR - RIG-I like receptors

RNP- Ribonucleoprotein

SAMHD1 - SAM domain and HD domain-containing protein 1

STAT - Signal Transducer and Activator of Transcription proteins

STING - Stimulator of interferon genes

TBK-1 - Tank Binding Kinase 1

TIR - Toll-Interleukin receptor

TLR - Toll like receptor

TNFα - Tumour necrosis factor Interferon beta

TREX1 - Three prime repair exonuclease 1

TRIF - TIR domain-containing adaptor protein inducing IFNβ

Acknowledgments

I would like to express my sincere gratitude towards my esteemed supervisor, Dr. Shovamayee Maharana, for her unwavering support, guidance, and mentorship throughout my academic journey. I extend my thanks to my esteemed expert Dr. Kundan Sengupta for his invaluable inputs during the midyear presentation, and to my co-supervisor, Dr. Nikhil Gandasi, for their consistent feedback, support, and innovative ideas on how to approach the project. I would like to express my gratitude to the members of my laboratory for their suggestions and discussions. I encountered several technical challenges while standardizing my work in a new laboratory. However, my senior, Ms. Shobha Elangovan provided me with exceptional troubleshooting protocols, for which I am grateful. I am thankful to Padmanava DasGupta for helping with this project and Prerna Narwal for the fruitful discussions. I extend my thanks to Prarthana Ghosh Dastidar and Anuva R., for their welcoming demeanor that made them approachable. Additionally, I extend my appreciation to my friend Saksham Rohilla, who generously assisted me with quantifications and analysis. I thank Dr. Subrata Ghosh, IIT Mandi, for providing us with RNA-select dyes, and Dr. Sachin Kotak, IISc, for providing us with HeLa Kyoto cells. Finally, I extend my profound appreciation to my family members for their unwavering support, without which this study would not have been possible.

Contributions

Contributor name	Contributor role
Dr. Shovamayee Maharana	Conceptualization Ideas
Dr. Shovamayee Maharana	Methodology
Dr. Shovamayee Maharana	Software
Dr. Shovamayee Maharana	Validation
Aishwarya Juneja, Saksham Rohilla	Formal analysis
Aishwarya Juneja, Padmanava DasGupta, Dr. Shovamayee Maharana	Investigation
Dr. Shovamayee Maharana	Resources
Aishwarya Juneja	Data Curation
Aishwarya Juneja	Writing - original draft preparation
Dr. Shovamayee Maharana, Lab members, Aishwarya Juneja	Writing - review, and editing
Dr. Shovamayee Maharana, Aishwarya Juneja	Visualization
Dr. Shovamayee Maharana	Supervision
Dr. Shovamayee Maharana	Project administration
None	Funding acquisition

This contributor syntax is based on the Journal of Cell Science CRediT Taxonomy[1].

[1] https://journals.biologists.com/jcs/pages/author-contributions

Abstract

The innate immune response in mammalian cells is a primary defense mechanism against pathogen invasions. The activation of highly sensitive sensors called pattern recognition receptors (PRRs) precedes the initiation of the innate immune response pathway. The PRRs detect pathogen or danger-associated molecular signatures. A subset of PRRs recognizes nucleic acids and signals the Type-I IFN response pathway, leading to the upregulation of inflammatory cytokines. This study investigates the effect of introducing DNA vectors and other nucleic acids in mammalian cells on the Type-I IFN response pathway and the activation of an antiviral pathway mediated by RNase L. We report the formation of nucleic acid assemblies within cells upon introducing nucleic acids. These assemblies contain DNA and are rich in RNA, and have not been previously described. Our findings demonstrate that the introduction of nucleic acids upregulates Type-I IFN genes and enhances RNase L levels, providing insight into the mechanism of nucleic acid-mediated immune responses.

Introduction

1.1 The nucleic acid sensing pathways

Humans encounter a diverse range of pathogenic invasions on a daily basis. Our ability to fight against the pathogen depends on the rapid detection of the infectious agent and quick induction of the appropriate defense response. Innate immunity is the primary line of the defense system in our bodies. It comprises physical barriers like skin and mucosal epithelia in various respiratory, reproductive, and digestive organs. However, a large number of parasitic microorganisms are evolved to override these physical barriers, enter our cells and cause infection. The first step towards fighting against pathogens and their associated diseases is detecting foreign agents. There are various intracellular receptors called pathogen recognition receptors (PRRs) that can detect specific conserved motifs or structures encoded in microorganisms called pathogen-associated molecular patterns (PAMPs) (Janeway, 1989). The detection of PAMPs, or self-derived danger signals called DAMPs (danger-associated molecular patterns), by the PRRs leads to an activation of the innate immune response pathway. Some pathogenic biomolecular signatures that can act as PAMPs are peptidoglycans, lipoproteins, etc. (Silva-Gomes *et al.*, 2014) that comprise microbial envelopes. Others include microbial nucleic acids or their genomes. In the case of virus-like pathogens, nucleic acid becomes an important PAMP for eliciting an immune response pathway (Chow *et al.*, 2018).

Several PRRs (Figure 1) are known to detect foreign nucleic acids like cyclic GMP-AMP synthase (cGAS) (Shu *et al.*, 2014; Webb and Fernandez-Sesma, 2022), RIG-I-like receptors (RLRs) (Kang *et al.*, 2002; Yoneyama *et al.*, 2004), nucleotide oligomerization domain (NOD) (Girardin *et al.*, 2003a, 2003b) like receptors and toll-like receptors (TLRs) (Rock *et al.*, 1998; Hemmi *et al.*, 2000; Pelka *et al.*, 2016). These are mainly classified based on the type of nucleic acids they detect- DNA, ssRNA, dsRNA, DNA-RNA hybrid, and both DNA and RNA (Kawasaki *et al.*, 2011). The host cells also have abundant nucleic acids in their cytoplasm, so how do the PRRs escape detection of self-nucleic acids? It is majorly dependent on structure, availability, and localization. Self-nucleic acids are degraded rapidly by nucleases before they encounter PRRs and lead to false sensing (Schlee and Hartmann, 2016). Various

receptors like RLRs recognize 5'- triphosphosphates and 5'-diphosphates present in ssRNA and dsRNA of the viral genome (Goubau *et al.*, 2014). Other ways include using enzymes like ADAR1 (adenosine deaminase) that deaminates adenosine to inosine (Savva *et al.*, 2012). Engagement of PRRs with PAMPs triggers intracellular signaling cascades that culminate in the expression of various proinflammatory molecules and type-I interferons. The proinflammatory cytokines include interleukin-1 (IL-1), interleukin-6 (IL-6), etc. They are known to induce several events, along with inflammation and activation of B and T cells, involved in adaptive immunity.

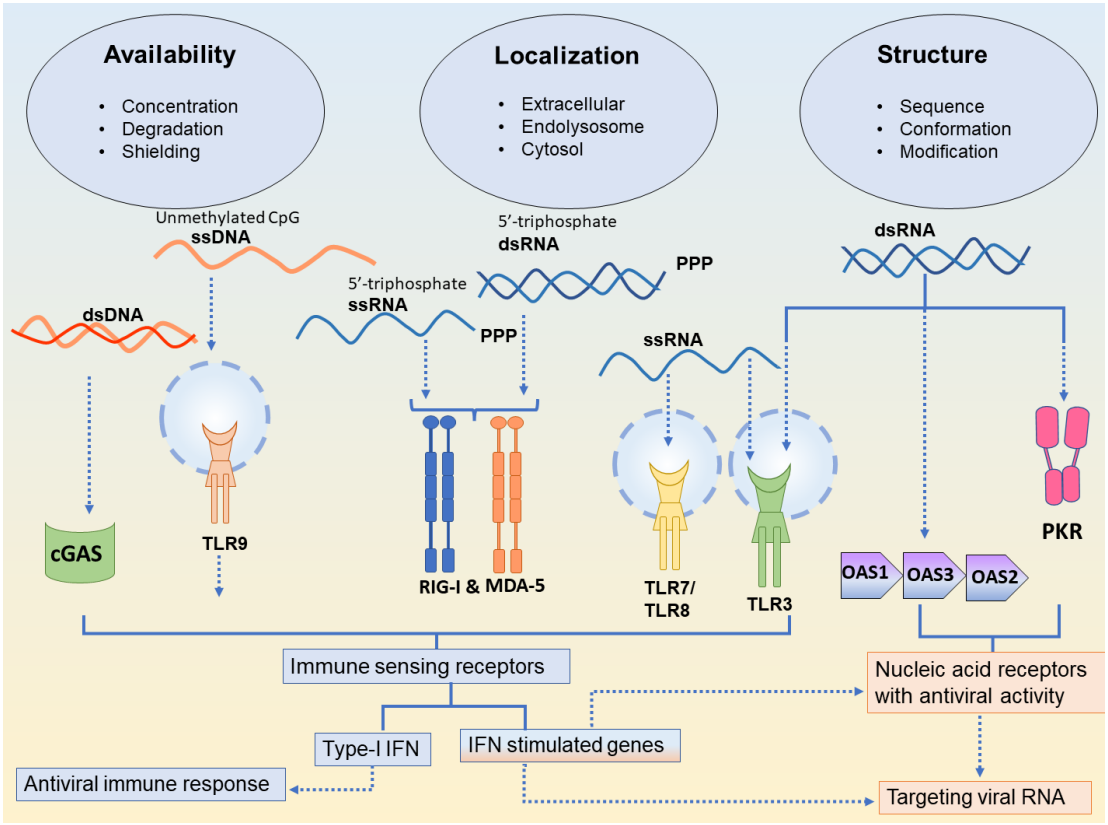

***Figure 1: PRRs and their categories*.** The figure depicts the principal basis of the detection of self-versus non-self-nucleic acids. It primarily depends on nucleic acid availability, its localization, and its structure. The more available and abundant self-nucleic acids are rapidly degraded by nucleases. The localization and structure determine which PRR would interact with the given nucleic acid. The PRRs initiating an immune response include TLRs in endolysosomes and RIG-I, MDA5, and cGAS in the cytoplasm. TLR7 and 8 detect ssRNA, and TLR3 detects ss and dsRNA in the endolysosome. TLR9 detects ssDNA containing unmethylated CpG motif. RIG-I and MDA5 detect cytosolic dsRNA, and cGAS detects cytosolic dsDNA. Other receptors, like OAS, PKR, etc., detect dsRNA and exhibit direct antiviral activity. They are also activated by IFN-stimulated genes.

Modified from (Schlee and Hartmann, 2016)

1.1.1 DNA sensing receptors

DNA sensing receptors like AIM2, cGAS, and TLR9 can activate the innate immune response (Schlee and Hartmann, 2016). However, the PRRs of interest for this study are cGAS and TLR9 due to the difference in their localization. cGAS is a cytosolic PRR, while TLR9 is enclosed in an endolysosome (Figure 1).

The Cyclic GMP-AMP synthase (cGAS) is a type of PRR involved in detecting cytosolic dsDNA, whether self or foreign. Once dsDNA is detected, cGAS binds to it and produces cyclic GMP-AMP (cGAMP), a second messenger molecule (Li *et al.*, 2013; Wu *et al.*, 2013). cGAMP attaches to the transmembrane protein stimulator of interferon genes (STING), located in the endoplasmic reticulum, and activates it, leading to its translocation to intermediate compartments between the endoplasmic reticulum (ER) and Golgi (Ishikawa and Barber, 2008; Ishikawa *et al.*, 2009). During translocation (Guo and Novick, 2004), TANK-binding kinase-1 (TBK1) is recruited by cGAMP, resulting in the phosphorylation of STING. This, in turn, leads to the recruitment of interferon regulatory factor-3 (IRF3) (Shu *et al.*, 2014). IRF3 is also phosphorylated by TBK1, leading to its dimerization. The complex then moves to the nucleus, enhancing the transcription of genes responsible for producing various cytokines, chemokines, and interferons (Figure 3). Furthermore, Iκβα, an inhibitor of the transcription factor NF-κB, is phosphorylated by TBK1, thereby targeting it for proteasomal degradation (Chien *et al.*, 2006). The Iκβα degradation releases NF-κB, allowing it to move to the nucleus together with IRF3, where they work synergistically to combat invading pathogens.

Other immune sensing receptors include TLRs. The TLRs are formed in the endoplasmic reticulum (ER) and are transported to the Golgi apparatus. From Golgi, they are eventually recruited to membranous compartments, such as endosomes, involved in the Golgi trafficking pathway. The TLRs need different proteins to help them mediate from ER to the endosome (Okude *et al.*, 2021). TLR9 requires an adaptor protein 2 (AP-2) complex that aids in endocytosis from the cell membrane to endosomes (Lee and Barton, 2014). TLR9 recognizes CpG-motif-containing ssDNA in the endolysosomal compartment (Hemmi *et al.*, 2000). There are two binding sites- N terminal leucine-rich-repeat (LRR) cluster site and the C-terminal LRR cluster site, that enable ligand-mediated dimerization of TLR9 (Miyake *et al.*, 2018), which leads to the activation of downstream signaling pathways and trigger an immune response

that includes the production of interferons and B cell activation. Chromosomal and mitochondrial DNA are dsDNA; therefore, they must be broken down into small, single-stranded fragments before they can bind to TLR9. The lysosomal DNase, known as DNase II is necessary for processing DNA to enable TLR9 to detect it (Miyake *et al.*, 2018). Cytosolic DNA is generally considered a danger signal that indicates the presence of non-self or damaged DNA, such as that from viruses or cancer cells. Other pattern recognition receptors, such as AIM2 (Hornung *et al.*, 2009), also recognize cytosolic DNA and activate similar immune responses. TLR9 can also detect cytosolic DNA under certain circumstances, such as when the DNA is complexed with antimicrobial peptides or when there is lysosomal damage that leads to the leakage of DNA into the cytoplasm.

1.1.2 RNA sensing receptors

Owing to the fact that majority of the viruses contain RNA as their genome, RNA sensing receptors are widely known due to their partake in activating antiviral pathways upon sensing viral genomic RNAs. Among, immune sensing receptors like TLRs detect RNA in endosomes and lysosome-related organelles (LROs) and RIG-I and MDA5 detect dsRNA in the cytoplasm (Figure 1). The nucleic acid receptors with antiviral activity include oligoadenylate synthase (OAS) and RNA-dependent Protein Kinase (PKR) sense dsRNA in the cytoplasm and activates RNases. These receptors are further stimulated by IFN stimulated genes (ISGs) (Figure 1).

TLR3 and TLR7 detect dsRNA within the endosome, and ssRNA is detected by TLR7 and TLR8 (Kawai and Akira, 2010; Greulich *et al.*, 2019; Kawai). The sensing via these receptors activates interferon (IFN)-regulatory factor 3 (IRF3) and IRF7 and trigger type-I interferon production by interacting with myeloid differentiation primary response protein 88 (MYD88) and TIR domain-containing adaptor protein inducing IFNβ (TRIF) (Kawai and Akira, 2010).

In the cytosol, helicases retinoic acid-inducible gene I (RIG-I) and melanoma differentiation-associated gene 5 (MDA5) recognizes dsRNA and transmit signals through mitochondrial antiviral signaling protein (MAVS) to generate type I interferon (Kang *et al.*, 2002; Yoneyama *et al.*, 2004; Chow *et al.*, 2018).

Oligoadenylate synthase (OAS) is a family of enzymes stimulated by ISGs (Pebernard and Iggo, 2004), involved in antiviral pathways. Upon detecting viral infection, OAS is upregulated and catalyzes the synthesis of 2'-5'-oligoadenylate (2-5A) molecules by polymerizing ATP molecules (Bisbal and Silverman, 2007; Takeuchi and Akira, 2010). The synthesized 2-5A molecules then bind to and activate RNase L by inducing its dimerization and subsequent conformational changes. The activated RNase L subsequently cleaves viral and cellular RNAs at specific sequences, leading to the inhibition of viral replication and spread (Huang *et al.*, 2014). Among OASes, OAS3 was reported to bind to dsRNA, synthesizing 2′,5′-oligoadenylate (2-5A) thereby leading to the dimerization and activation of RNase L (Li *et al.*, 2016).

RNA-dependent Protein Kinase (PKR) is another PRR involved in antiviral pathway, that upregulates and activates RNase L in response to viral invasion. PKR is synthesized in a quiescent, unphosphorylated state within the cell. Its activation and autophosphorylation are elicited upon binding to specific host- or pathogen-derived RNAs or through interactions with the protein activator of protein kinase R (PACT). Once activated, PKR phosphorylates eukaryotic initiation factor 2α (eIF2α), instigating the inhibition of protein synthesis constituting a crucial antiviral mechanism (Jha *et al.*, 2011; Husain *et al.*, 2012).

The activation of antiviral mechanisms via the sensing of PRRs ends up activating type-IFN response signaling innate immune response pathway.

1.2 Mechanistic understanding of type I-IFN induction

When type I interferons bind to IFNAR1 and IFNAR2 receptor subunits, it triggers the activation of kinases. These kinases then phosphorylate STAT1 and STAT2 proteins, leading to the formation of the ISGF3 (interferon-stimulated gene factor 3) complex (Honda *et al.*, 2005). The ISGF3 complex enters the nucleus and binds to ISREs (interferon-stimulated response elements), which activates the transcription of interferon-stimulated genes (ISGs) like PKR, OAS, and Mx protein, which inhibit viral replication and modulate cellular processes involved in antiviral response, immune regulation, cell growth, and apoptosis (Keating *et al.*, 2011).

1.2.1 Type-I interferonopathies, its consequences and the causal agents.

The monogenic type I interferonopathies are associated with a failure of self-versus non-self discrimination of nucleic acids by the PRRs due to mutations in one or many genes associated with the nucleic acid metabolism pathway. As of now, 38 Mendelian genes are associated with type I interferonopathies (Crow and Stetson, 2022). Most of them are nucleases like ribonuclease H2 (RNase H2 encoded by RNase H2A, RNase H2B and RNase H2C), SAMHD1, a dNTPase that may play a role in DNA repair, and TREX1, a DNase that degrades ss and dsDNA. Due to dysfunction of these genes, there is a constitutive Type-I IFN response leading to chronic inflammation in the bodies of affected individuals. One such autoinflammatory disorder called Aicardi Goutières Syndrome (AGS) involves mutation in SAMHD1 which was shown to act as an RNase recently (Maharana *et al.*, 2022). The study reported the sequestration of immunostimulatory dsRNA in membraneless, phase separated condensates in healthy individuals preventing aberrant type-I IFN response. However, in AGS patients, due to the deficiency of SAMHD1, dsRNA was not degraded, and the dsRNA could not be sequestered in the condensates. Eventually, the immunogenic dsRNA was released into the cytoplasm and upon interacting with RIG-I and MDA5, Type-I IFN response was activated leading to express inflammatory cytokines constitutively.

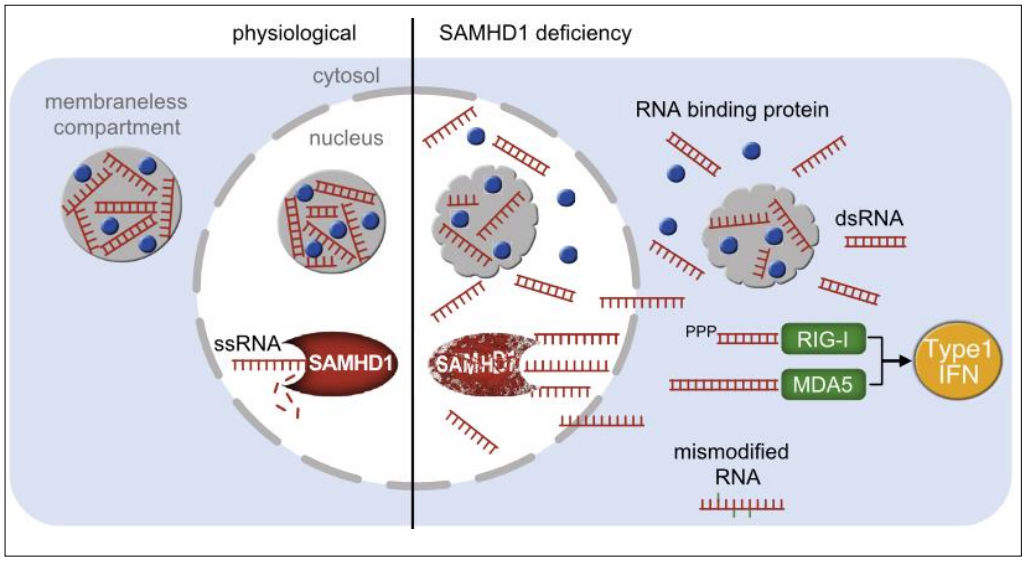

Figure 2: Constitutive Type-I IFN expression due to SAMHD1 deficiency. In physiological condition, the immunostimulatory dsRNA gets sequestered in membrane-less compartments and is subsequently degraded by the activity of SAMHD1. In AGS patients with a mutation in SAMHD1, the dsRNA is found to be released from the membraneless condensates in the cytoplasm, triggering an innate immune response and aberrant activation of Type-I IFN response.

Adapted from (Maharana et al., 2022)

1.2.2 The role of biomolecular condensates in innate immune response

A large number of membrane-bound organelles in the cells are involved in various biological functions. Endosomes, lysosomes, and related organelles are well known for their functions in immune response signaling. The Golgi trafficking pathway translocates nucleic acids, signaling factors, proteins, etc. in the cells. TLRs are enclosed in endolysosomes (Lee and Barton, 2014). However, eukaryotic cells also have membrane-less condensates (Banani *et al.*, 2017) that are formed by the process of liquid-liquid phase separation (LLPS). LLPS is a fundamental phenomenon where a homogenous solution of molecules demixes into two distinct liquid phases, each with different solute concentrations. These condensates perform various biological functions and are often hubs of nucleic acids. Studies have shown that these condensates have a propensity to sequester PRRs (Xiao *et al.*, 2022), and immunogenic nucleic acids (Paget *et al.*, 2021). One such study showed the formation of cGAS condensates (Du and Chen, 2018).

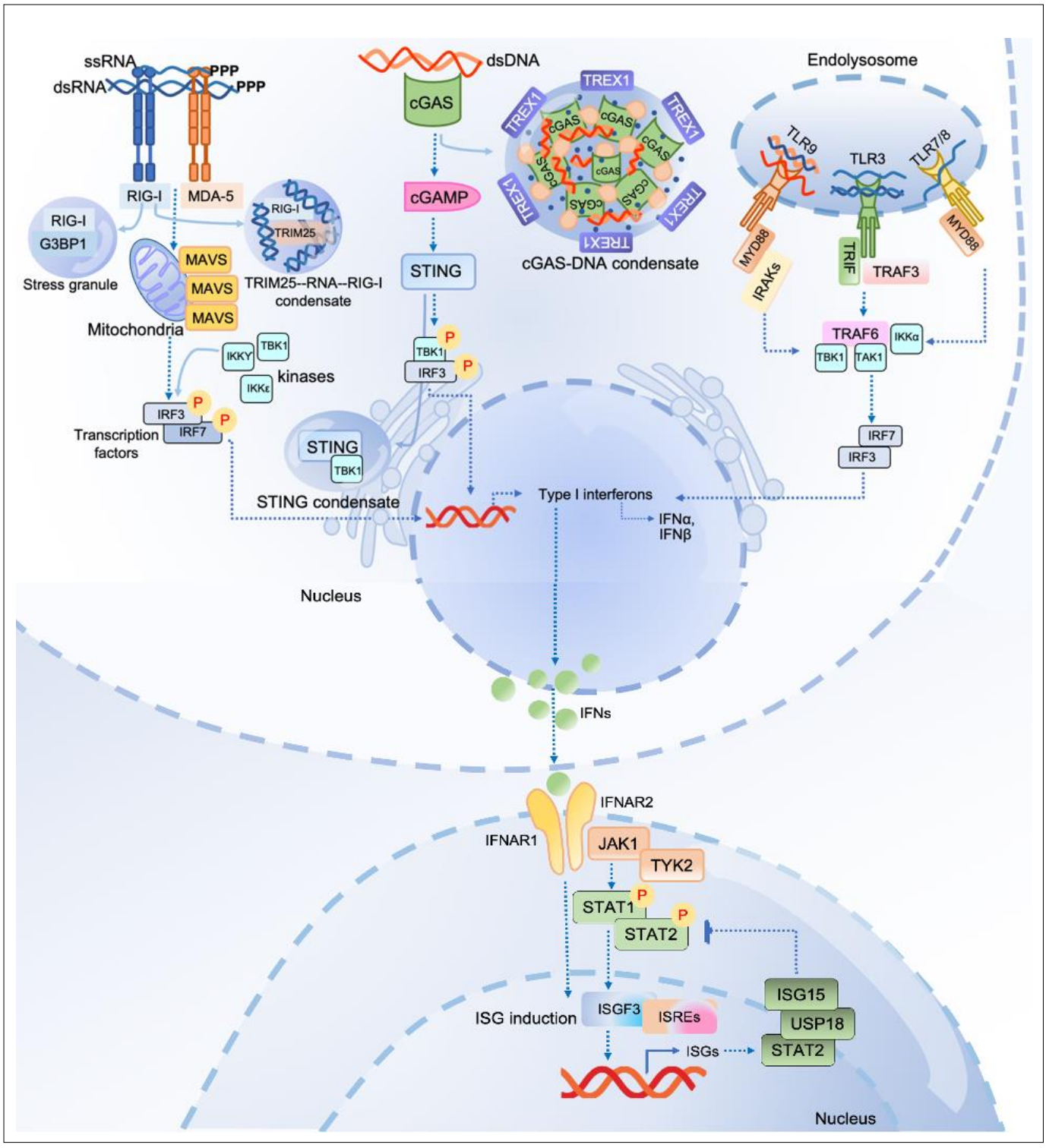

Figure 3: The condensates involved in immune sensing and nucleic acid recognition pathway. The figure depicts the nucleic acid signaling pathway via various receptors and the condensates involved in the process. RIG-I is sequestered into stress assemblies along with other stress assemblies proteins like G3BP1 etc. RIG-I also recruits TRIM25 to form a TRIM25-RNA-RIGI condensate. cGAS, along with dsDNA, recruits TREX1, a nuclease, and forms a condensate. The propensity of cGAS to form a condensate increases with zinc and streptavidin (produced during bacterial infections). cGAS leads to STING activation, and STING recruits kinases like TBK1 to form a condensate. TLRs, to begin with, are enclosed in endolysosomes and other lysosomal-related organelles. All the pathways lead to the production of type-I interferon response and upregulate cytokines. The cytokines then signal other cells and activate the JAK-STAT signaling pathway and upregulate various interferon-stimulated genes (ISGs).

1.3 The role of nucleases on immunogenic nucleic acids

The condensates mentioned above contain nucleic acids and the condensates involved in enhancing the inflammatory response (Figure 3) recruit nucleases to degrade and cleave potential immunogenic nucleic acids. Various studies have elicited the importance of DNases and RNases that could alter nucleic acid metabolism and cause heightened immune response. Some of the general ribonucleases, like RNase L and RNase T2 are of utmost importance as they are activated in response to an antiviral pathway (Chakrabarti *et al.*, 2012; Wu *et al.*, 2020).

These ribonucleases are dependent on PRRs. Prior to RNase L activation, the OAS3 domain gets activated upon sensing dsRNA (discussed in 1.1.2). The OAS/RNase L pathway is partially responsible for the inhibition of viral infections by interferons (IFNs). The dimerization and activation of RNase L lead to the cleavage of viral nucleic acids, thereby preventing viral replication (Li *et al.*, 2016). The cleavage of the viral genome leads to the formation of small transcripts with 5'-diphosphates and 5'-triphosphates, which are then sensed by RIG-I and MDA-5 in the cytosol, further activating Type-I IFN response. This leads to positive feedback as OAS, one of the ISGs now gets upregulated (Malathi *et al.*, 2007).

Another PRR that can initiate antiviral signaling and upregulate inflammatory cytokines is cGAS. The sensing of dsDNA by cGAS leads to the activation of type-I IFN response initiating the JAK-STAT signaling pathway. The induction of IFN signaling upregulates ISGs, like OASes, thereby leading to RNase L activation indirectly.

A recent study reported that the introduction of DNA vector through transfection activates the cGAS-STING pathway and elicits an immune response and suppresses transgene expression in the cells (Fu *et al.*, 2020). The IFN production leads to the signaling and upregulation of ISGs. This leads to the activation of RNase L and causes the degradation of RNAs, altering RNA metabolism.

1.4 Hypothesis and Objectives

Using the above-mentioned information as a premise, we hypothesize that transfection of the DNA vectors in the cells leads to activation of RNase L and elicits Type-I innate immune response. The upregulation of ISGs through the RNAi mechanism has already been reported (Bridge *et al.*, 2003; Pebernard and Iggo, 2004). However, the downstream signaling and the effect of the activation of RNases on RNA metabolism have been overlooked.

In order to study the impact of transfection on RNA metabolism, we have developed a model. Our approach involves transfecting HeLa cells with different types of nucleic acids, followed by quantifying the overall RNA level. We measure the expression of type-I IFN and RNase L gene levels and investigate the altered nucleic acid metabolism and localization in mammalian cells.

We speculate that the altered nucleic acid metabolism is caused due to the activation of cGAS-STING pathway upon transfection with plasmid vectors. We have a synthetic dsRNA, Poly I:C, as a positive control.

Chapter 2 Materials and Methods

2.1 Plasmid isolation:

From ~30mL of culture, the plasmids were isolated using Qiagen miniprep kit (Cat#27104) for transfections. The instructions were followed as per the kit and the buffer volumes were scaled according to the volume of the cultures. The DNA was eluted using nanopore water instead of elution buffer. To check the quality of the DNA, nanodrop readings were taken, and the plasmids were run on the gel.

2.2 Gel electrophoresis:

To check the purity of the plasmids, we ran 500ng DNA on 0.8%-1% agarose gel in 1X TAE buffer at 100V. The gel was visualized under UV using Biorad gel doc equipment. For running RNA gel, we loaded 500ng RNA on a 1% agarose gel and used 1X TBE buffer at 100V.

2.3 Cell Culture:

HeLa Kyoto cells were maintained at 37°C, 5% CO_2 in high glucose (4.5gm/liter) DMEM (Himedia, AT068) with 5% FBS (Himedia, catalog number) and 1X PenStrep. PC12 cells were maintained at 37°C/5% CO_2 in modified DMEM, Horse serum (25 U/ml) Fetal Bovine Serum (25 U/ml), and Pen Strep (5 U/ml) (Life Technologies, USA). Passaging/subculturing all types of cells: The cells were washed with 1X PBS, trypsinized using 0.25% Trypsin-EDTA (Himedia, catalog number), kept in the incubator for 2-3 mins and the trypsin was neutralized using fresh DMEM containing 5% FBS and 1X PenStrep (complete DMEM). The suspension was then transferred to 15mL centrifuge tubes and were pelleted down at 1200 rpm. The media with trypsin was then removed and the pellet was resuspended in complete DMEM and added in flask. HeLa Kyoto cells were a gift from Dr. Sachin Kotak, MCB dept, IISC, and PC12 cells were kindly given by Dr. Nikhil Gandasi, MRDG, IISc.

2.2 Transfection and Treatments:

Plasmids (addgene/alberti lab) or poly(I:C) (Invivogen, tlrl-pic) were transfected using PEI (polycation polyethyleneimine) for all cell types. Transient transfections were

performed on 12-mm coverslips in 24-well plate for imaging experiments and in 6-well plates for RNA isolation. The transfection mix comprised of 50/100 µL OptiMEM (Gibco, 31985-070) using 3/6µL Polycation Polyethyleneimine (PEI), 1µg/2µg nucleic acids (PEI:DNA = 3:1). After 5-6 hours, the medium was replaced with complete DMEM., after transfection followed by imaging/RNA isolation. The imaging was performed after 24 hrs and the cells for RNA isolation were harvested in RNAisoplus 6 hrs after replacing the media. The plasmids used were pSICOR-sh-Scrambled-CMVmcherry coding for a scrambled shRNA sequence (5'-GCAACAAGATGAA GAGCACCAA-3'), cloned in Maharana et al.,2022; pH2B-mcherry-IRES-neo3 (addgene), pLKO.1-puro-sh-Scrambled and pENTR-SRSF2 (made using gateway cloning by Padmanava DasGupta). For all transfections, $6*10^4$ cells were plated on 12mm coverslips in a 24-well plate for RNA staining/ immunofluorescence staining or $0.2*10^6$ cells in 6-well plates for RNA isolation. For conditioned media experiment, after 5-6 hrs of transfection, the media was replaced with fresh DMEM and after 6 hrs, the conditioned media was then transferred to untreated cells. The cells were treated with conditioned media for 6 hrs and were then fixed/harvested for staining/RNA isolation respectively.

2.3 Immunofluorescence:

The cells were plated on 24-well on coverslips and treated the next day with the transfection mix. After following usual transfection protocol, the cells were fixed with 4% formaldehyde in 1X PBS, pH 7.4. This was followed by 1X PBS washes, 3 times. After fixation, 10-minutes permeabilization was performed using 0.25% Triton-X-100 in 1X PBS followed by 3 PBS washes and blocking in 2% BSA (MP Biomedicals, 160069) made in 1X PBS for 4-6 hrs. After 3 washes, primary antibody- G3BP1 (CST, 61559, epitope: Against residues surrounding Val218 of human G3BP1 protein, rabbit, monoclonal) in a 1:1000 dilution, made in 2% BSA was added and the coverslips were left in the hydration chamber at 4 degrees overnight. Next morning, the coverslips were washed thrice and were incubated in secondary antibody (Anti-rabbit Alexa Fluor 555) in a 1:1000 dilution for 2-3 hours at RT After washing with PBS thrice, the coverslips were stained with DAPI (1:1000 dilution in 1X PBS), incubated at RT for 10 mins and this was followed by RNA staining using 500nm RNAselect dye (Thermofisher, catalog number) for 20 mins. The coverslips were then mounted on glass slides using antifade solution. Images were taken immediately within 30 mins after staining.

2.4 Staining and Imaging:

For both transfection and Immunofluorescence assay studies, the supernatant was removed from the cells, and they were washed twice with 1X PBS. They were then fixed with 4% formaldehyde made in 1X PBS for 10 mins at RT and washed thrice. This was followed by 10 mins DAPI (1:1000 dilution) staining and RNAselect (Thermofisher, absorption/emission maxima ~490/530nm) staining (500nm) for 20 mins to stain for RNA or 5μM Thr1 (kindly gifted by Dr Subrata Ghosh, I.I.T. Mandi). For WGA (kindly provided by Dr. Subba Rao, M.C.B., IISc) staining, the coverslips were incubated in 5μM of the solution made in 1X HBSS buffer for 20 mins and were then mounted on the glass slides using 2μL antifade solution. The imaging for the RNA dyes (both RNAselect and Thr1) were done in sets as the images need to be taken within 30 mins after staining else, they photobleach. The fluorescence images were taken in a wide-field Leica microscope (DMI6000B) using 63X and 100X objective lens. The immersion oil (Leica microsystems C.M.S. GmbH, 11513859) has a refractive index of 1.518 and viscosity (v_e) =46.

2.5 RNA isolation:

For RNA isolation, $0.2*10^6$ cells were seeded in a 6-well plate per well and allowed to adhere overnight with 5 % CO_2 at 37 °C. Post-treatment, cell culture supernatant was removed, and cells were washed with 1X PBS twice and stored at -80 degrees in 1 ml of RNA-iso plus (Takara, 9108/9109). RNA was extracted according to the manufacturer's instructions using the RNA-iso plus-chloroform extraction method.

For isolating RNA, the RNA-iso plus stocks kept in -80 degrees were thawed and to the solution, 0.2 ml of chloroform/1ml of RNA-iso plus was added and centrifuged at 12,000g for 15 min at 4°C. The solution was separated into three layers; top liquid layer (contains RNA), semisolid middle layer (mostly DNA), and bottom organic solvent layer. The top liquid layer was transferred to new microcentrifuge tube without touching the middle layer. Next, 0.5 to 0.6 ml or equal vol of isoproranol was added to the aqueous phase, mixed well and incubated 10 min at RT. The samples were then centrifuged at 12,000g for 10min at 4°C to pellet the RNA. The supernatant was removed and RNA pellet was washed with 75% cold ethanol by centrifuging the solution at 7,500g for 5 min at 4°C. The supernatant was discarded, and the pellet was dried by leaving the tube open for several min. RNA was then dissolved in 20uL of RNase-free water. This was followed by running 1ug of RNA on a 1% agarose gel

using 1X TBE buffer made in DEPC-treated water to check the quality of RNA samples.

2.6 cDNA synthesis:

500 ng of total RNA was used for cDNA conversion using PrimeScript™ cDNA Synthesis Kit (Cat#RR037A). Instructions were followed according to the kit. For a 10µL reverse transcription reaction, 0.5µL of PrimeScript RT Enzyme Mix I, 0.25 pmol of oligodT primer, 50 pmol of random 6-mer primer and 1X PrimeScript buffer was used.

2.7 Quantitative PCR:

Real-time analysis was done using Takara TB Green Premix Ex Taq II kit (catalog no: #RR820A) in 10 µl reaction volume as per manufacturer's instructions. Expression levels (Ct values) of GAPDH were used to normalize the expression data. Quant Studio 6 instrument and its corresponding software was used. Primers used for qPCR are mentioned in the table below. All the primers were obtained from Bioserve.

Primers	Sequence
Hu GAPDH Fwd	5' GTCTCCTCTGACTTCAACAGCG 3'
Hu GAPDH Rev	5' ACCACCCTGTTGCTGTAGCCAA 3'
Hu IFNβ Fwd	5' AAACTCATGAGCAGTCTGCA 3'
Hu IFNβ Rev	5' AGGAGATCTTCAGTTTCGGAGG 3'
Hu RNase L Fwd	5' AAGGCTGTTCAAGAACTACACTTG 3'
Hu RNase L Rev	5' CATCAAGTGGGCTGGAGATCCA 3'

Table 1: The sequence of primers used for qRT-PCR analysis. 0.4µM of each primer was used.

2.8 Quantification and Statistical Analysis:

Microscopy: The raw folders were retrieved and moved to one folder using a basic MATLAB move files code. The images were then split and among the z-stacks, the best focused z-projection was analysed. The cell boundary as region of interest (ROIs) around the cells were drawn and a mask was created. The mean cytoplasm intensity was calculated for each cell within this mask. Using colour thresholding of the DAPI and RNA channel, the nucleus, nucleolus and the assemblies mask were made (the code was modified from Maharana et., al 2022). For the nucleic acid assemblies quantification, the number of assemblies in each cell and the fraction of cells showing the assemblies were counted using an ImageJ plugin counter. The total number of cells and assemblies from each image was taken as each sample and the mean and standard deviation across the images were plotted. Similarly the co-localized assemblies were manually counted and plotted.

qRT-PCR: The CT values were obtained for our genes and the control- GAPDH. ΔCT was obtained by subtracting the CT value of the gene with the corresponding CT value of GAPDH for each sample. ΔΔCT for each sample was obtained by subtracting the respective ΔCT values from the average ΔCT of GAPDH of Mock sample. Using the ΔΔCT values, the fold change was calculated. Fold change $=2^{(-\Delta\Delta CT)}$.

For all graphs, Mean is plotted with SD as error bars from at least 3 technical replicates. The significance is quantified by two-tailed unpaired t-test (unequal variance).

Chapter 3 Results

3.1 Transfection of nucleic acid causes inflammation and activates Type-I IFN response

The expression of IFNβ was measured to check the inflammatory response and upregulation of cytokines upon transfection of nucleic acids. It is one of the crucial cytokines upregulated in Type-I IFN response. Plasmids (circular dsDNA) that code for ssRNA (pH2B-mCherry), dsRNA (pSICOR-nh-shRNA-mCherry), and synthetic dsRNA (Poly I:C) were transfected, and the inflammatory response was measured (Figure 4). We observed an enhanced inflammatory response by around ~100 folds upon treating the cells with nucleic acids. We observed that the cells treated with synthetic dsRNA showed higher IFNβ expression by ~130 folds compared to those treated with plasmid vectors. There was no significant difference in the expression levels in cells treated with an ssRNA coding plasmid and those treated with a dsRNA/shRNA coding plasmid.

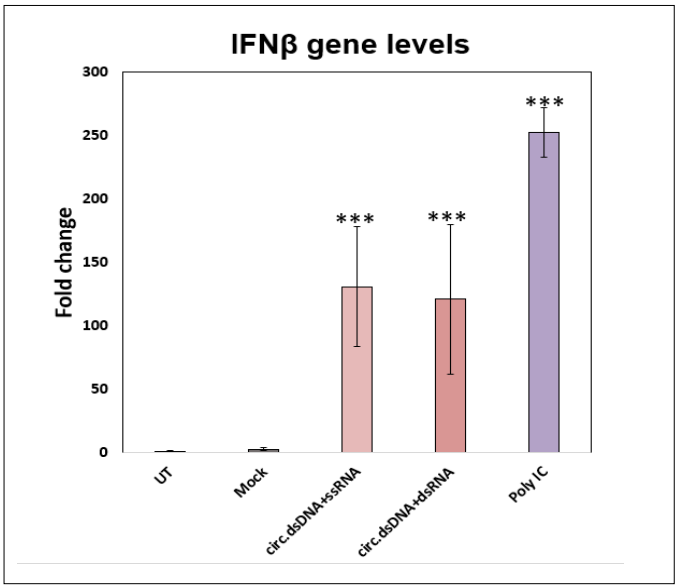

Figure 4: Expression of IFNβ gene levels using qRT-PCR. There is an increased expression of IFNβ in the treated cells. dsRNA treated cells show upregulation of IFNβ levels by ~130 folds. The fold change on the y-axis is 2^(-ΔΔCT). The inflammatory response was measure after 12 hrs of transfection

Error bars represent the SD of 3 technical replicates.

*Statistical test: Student t-test, ***p<0.0001, **p<0.05, non-significant (n.s.)*

From this data, we can conclude that transfection of all kinds of nucleic acid results in an upregulation of inflammatory response, and transfection of synthetic dsRNA lead to the highest IFNβ expression levels.

3.2 Upregulation of RNase L in the transfected cells

In antiviral, inflammatory response pathways, various RNases are activated in the downstream signaling pathways. PRRs with direct antiviral activity like OAS and PKR upregulate and activate RNase L (Jha *et al.*, 2011; Chakrabarti *et al.*, 2012; Li *et al.*, 2016). Upregulation of RNase L is also observed via the cGAS-STING pathway (Shu *et al.*, 2014; Webb and Fernandez-Sesma, 2022). To check if RNase L is indeed getting activated due to the transfection of nucleic acids, we measured RNase L gene levels. We found that there is undoubtedly an enhanced expression of RNase L by ~30 folds, and there is no significant difference among the treated samples (Figure 5). The expression levels of RNase L in plasmid vectors were comparable to synthetic dsRNA.

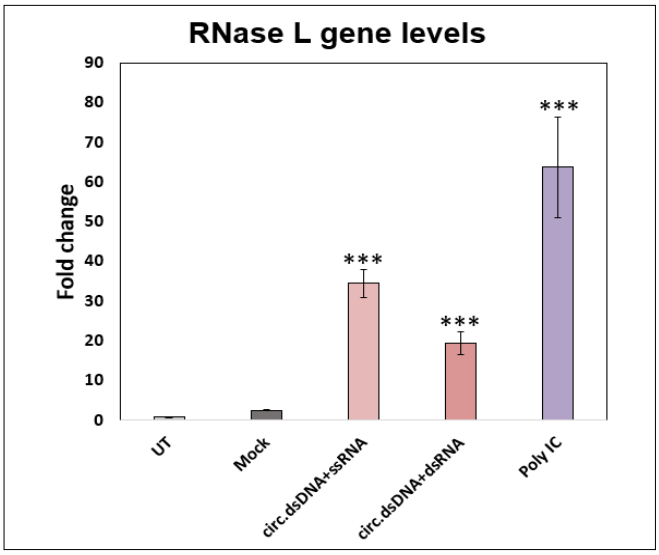

Figure 5: Expression of RNase L gene levels measured using qRT-PCR. The fold change is high for the treated wells. There is no significant difference between plasmid vectors and dsRNA. The fold change on the y-axis is 2^(-ΔΔCT). The response was measured 6 hrs after the treatment.

Error bars represent the SD of 3 technical replicates.

*Statistical test: Student t-test, ***p<0.0001, **p<0.05, non-significant (n.s.)*

From the above data, we conclude that transfection of nucleic acids leads to upregulation of RNase L. RNase L enhancement has been shown in Poly I:C transfected cells, but we observe that the plasmid vectors also cause an upregulation of RNase L levels to a similar extent.

Upon observing an increase in RNase L expression level, we speculated that RNase L is getting activated and leading to RNA degradation in the cells. To check if this is true and RNA is being degraded, we ran the RNA samples on a 1% agarose gel, and no evident degradation was observed in the treated samples (Figure 6).

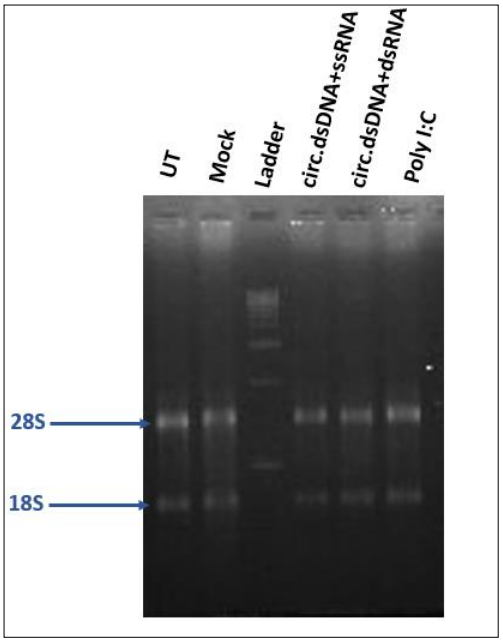

Figure 6: Checking degradation of RNA upon transfection. Upon running total isolated RNA on agarose gel, no degradation was observed in the transfected samples. ~500 ng of RNA was loaded in each lane.

The gel showed intact 28S, 18S, and 5S bands with no apparent degradation in treated wells. However, in this case, a gel is a crude way of quantification of total RNA levels. We were also curious about the localization of the RNA in treated cells. Thus, we performed staining experiments to quantify RNA level and check RNA localization.

3.3 Formation of nucleic acid assemblies upon transfection

3.3.1 Transfection of DNA vectors gives rise to nucleic acid assemblies

For RNA quantification, we used RNA select dye. It binds to RNA and stains the available RNA in the cells. DNA uptake is a random event, and not all the cells of the treated well have plasmid DNA. Therefore, the quantification of the transfected cells and those not transfected but exposed to the transfection mix (called untransfected here) was performed separately. Figure 7(B) shows no significant difference between the transfected and the untransfected cells. However, a ~40% decrease in the mean RNA select intensity in the cytoplasm and a ~35% decrease in the nucleoplasm of treated cells (transfected and untransfected taken together) compared to untreated cells was observed. No significant difference in the nucleolus intensity was observed. This data concluded that the RNA level is significantly lower in the cytoplasm and nucleoplasm of the treated cells. The decrease in the RNA intensity in the cytoplasm is also apparent from the microscopy images- LUT (lookup table) of the RNA channel (Figure 7(A)).

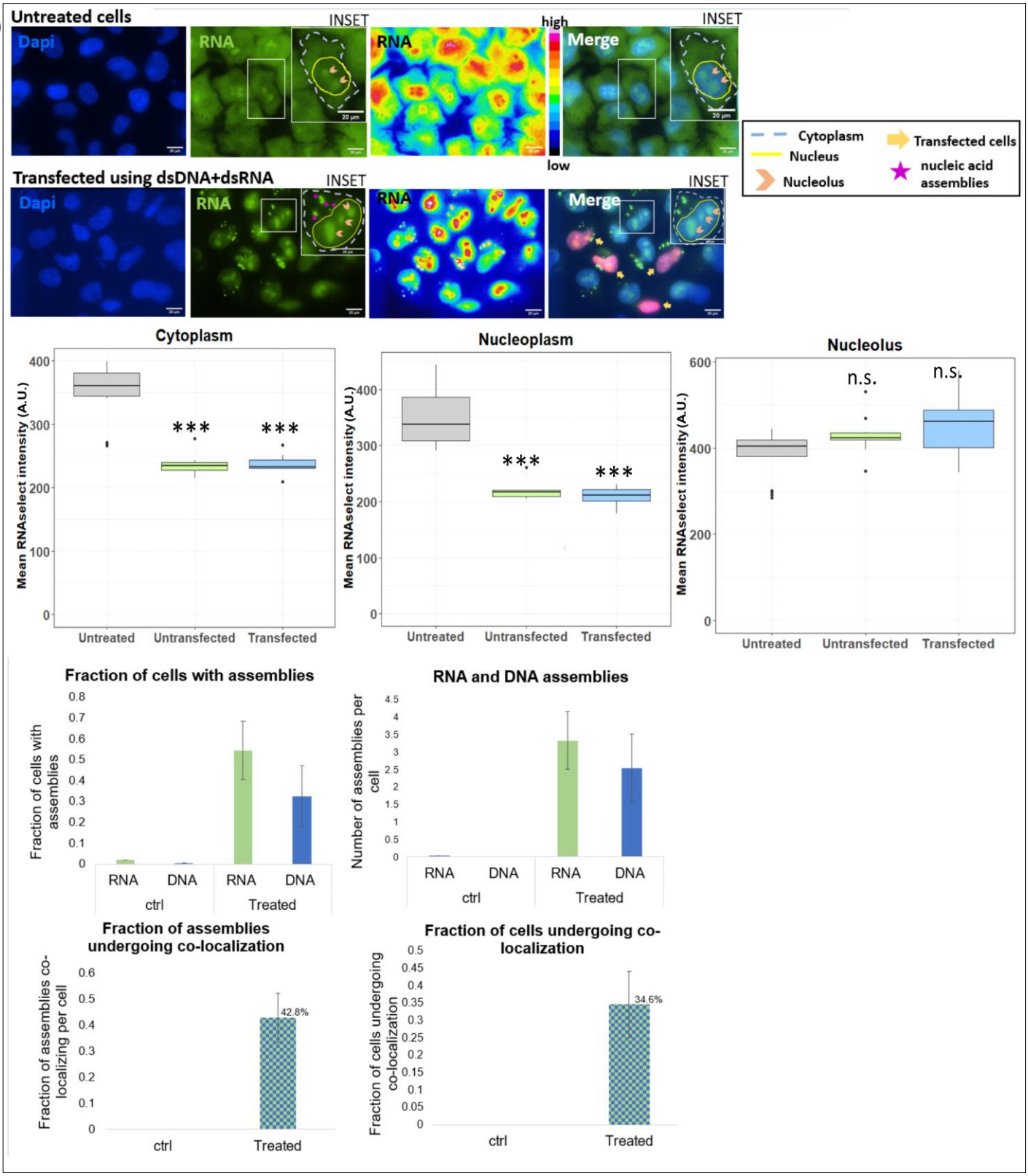

Figure 7: Transfection of a plasmid vector coding for dsRNA A) RNA and DAPI staining of the fixed coverslips shows DAPI and RNA assemblies. LUTs of RNA channels show the intensity map of RNA in the treated cells ranging from low (black) to high (white). B) Quantification of the RNA intensity levels in cytoplasm, nucleoplasm, and nucleolus. A significant increase in the intensity of untreated cells is seen compared to the treated cells. Treated cells include- transfected cells, the ones expressing mCherry

protein, and the untransfected ones that are not expressing mCherry protein. *n=23 untreated cells, 10 untransfected cells, and 8 transfected cells*. C) Quantification of the assemblies observed upon treatment. The number of RNA assemblies and the fraction of cells with RNA assemblies are ~20% more than DAPI assemblies. It is observed that around 35% of the cells undergo co-localization, and around 43% of assemblies are seen to co-localize. *n=202 control cells and n=194 treated cells*.

*Statistical test: Student t-test, ***p<0.0001, **p<0.05, non-significant (n.s.). Scalebar: 20μm.*

From the microscopy images, RNA localization seems altered in treated cells. RNA and DNA assemblies (Figure 7(A)) were observed in the cytoplasm of the treated cells. These assemblies were alike in the transfected and the untransfected cells. This could mean that the sensing of nucleic acids in itself is leading to the formation of these assemblies. The DAPI staining for these assemblies could explain the staining of DNA vectors, but we observed RNA foci too. We were curious to know if all of these assemblies had both DNA and RNA. Therefore, we tried to compute their number and check the co-localization of the assemblies.

To check the number of assemblies and the fraction of cells undergoing co-localization, we independently quantified RNA and DAPI assembly numbers. Then we checked for the number of assemblies co-localizing (Figure (C)). From these plots, we observe that ~50% of the cells show RNA assemblies and 32.4% show DAPI assemblies, and on average, ~3.5 RNA assemblies and 2.5 DAPI assemblies per cell were observed. From co-localization plots, we observe that 34.6% show co-localization and, on average, 42.8% of RNA assemblies per cell co-localized with DAPI assemblies.

To ensure that this is not an artifact of the dye, another RNA-binding dye was used called Thr1. As a negative control, the cells were treated with the transfection reagent and no plasmid (mock transfection). No assemblies in mock-transfected cells, and the assemblies were observed only in the treated cells (Figure 8 (A)) corroborating our observations with RNAselect dye. As observed from Figure 7, there was no significant difference in terms of mean intensity and assemblies among the treated cells. Hence, the cells were now treated with a tagless plasmid to ensure that this is not caused by overexpression of any protein. Another plasmid vector encoding for control scrambled shRNA (pLKO.1-puro-sh-Scrambled) with a different backbone was used.

Similar to our previous observations, we found a significant reduction in the RNA intensity of the treated cells in cytoplasm and nucleoplasm. In this experiment, we also saw significantly reduced intensity in the nucleolus of the treated cells (Figure 8(B)). The reduction in the intensity in the cytoplasm, nucleoplasm, and nucleolus was equivalent to ~35%. From this, we can conclude that there is indeed a reduction in RNA levels in treated cells as compared to mock-transfected cells.

The numbers of the observed DNA and RNA assemblies were measured, and the co-localization was quantified. ~60% of the assemblies per cell were shown to co-localize, and ~65% of the total cells were observed to depict assemblies that co-localize.

From the above experiments, we can conclude that there is an altered localization of RNA and/or a decrease of RNA is observed upon transfection. The nucleic acid assemblies were observed only in treated cells.

(A)

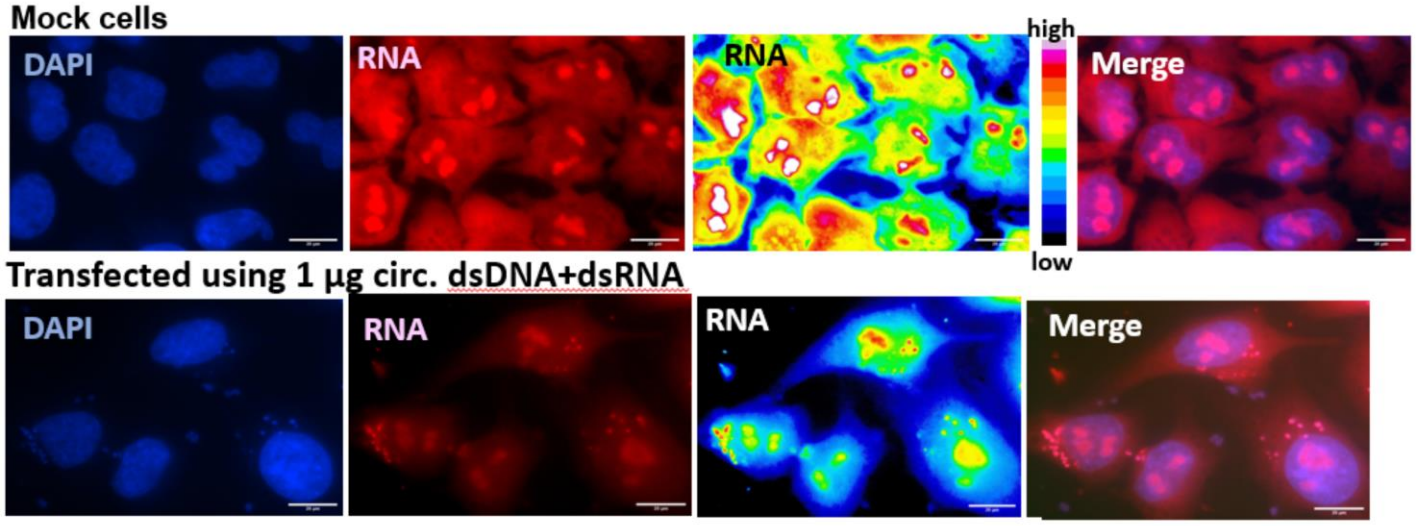
Mock cells
DAPI
RNA
RNA
high
low
Merge
Transfected using 1 µg circ. dsDNA+dsRNA
DAPI
RNA
RNA
Merge

(B)

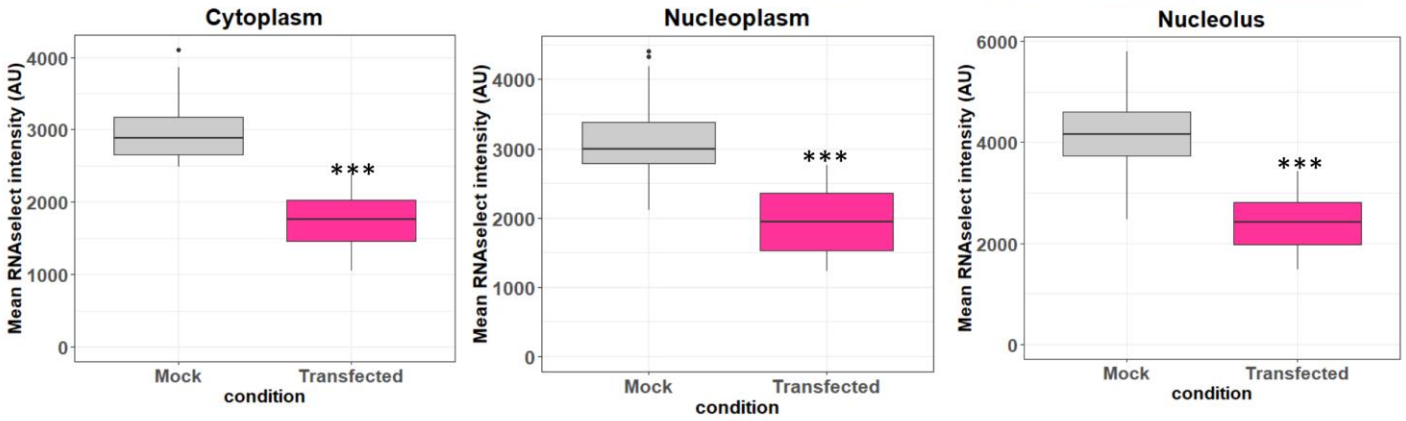
Cytoplasm
Nucleoplasm
Nucleolus
Mean RNAselect intensity (AU)
***
Mock
Transfected
condition

(C)

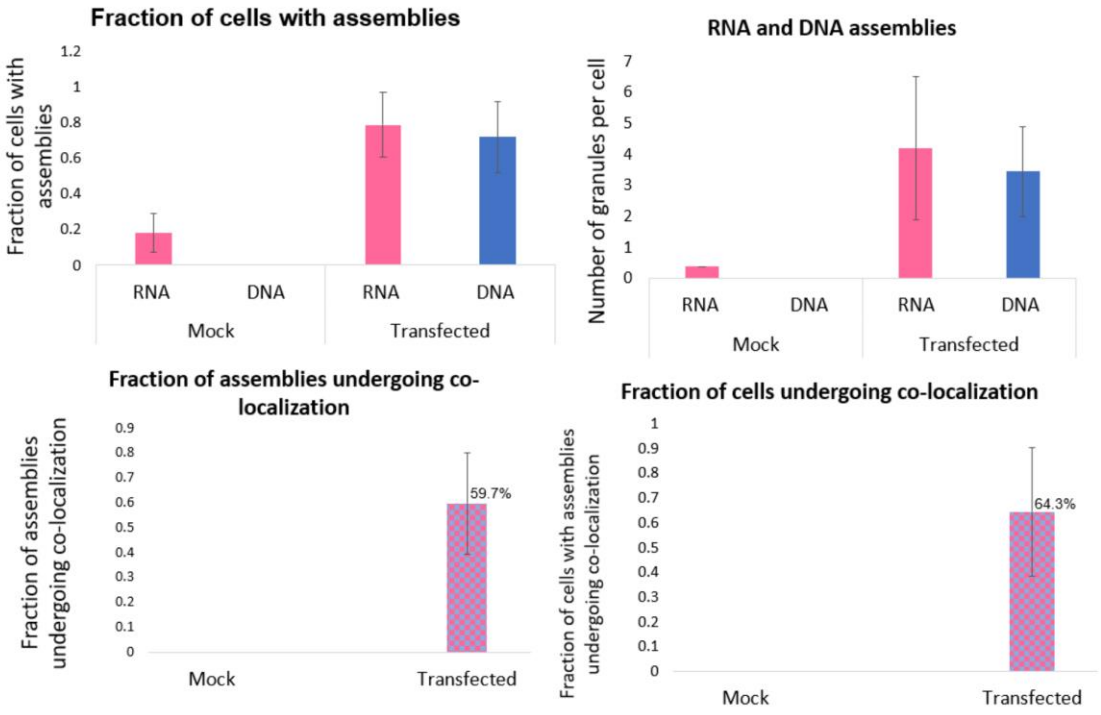
Fraction of cells with assemblies
Fraction of cells with assemblies
RNA
DNA
Mock
Transfected
RNA and DNA assemblies
Number of granules per cell
Fraction of assemblies undergoing co-localization
Fraction of assemblies undergoing co-localization
59.7%
Fraction of cells undergoing co-localization
Fraction of cells with assemblies undergoing co-localization
64.3%

Figure 8: Transfection of dsRNA encoding plasmid A) RNA staining with Thr1 dye of the fixed coverslips shows DAPI and RNA assemblies. LUTs of RNA channels show the intensity map of RNA in the treated cells ranging from low (black) to high (white). B) Quantification of the RNA intensity levels in cytoplasm, nucleoplasm, and nucleolus. A significant increase in the intensity of untreated cells is seen compared to the treated cells suggesting a global reduction in RNA levels. *n= 33 mock cells and 48 transfected cells*. C) Quantification of the assemblies observed upon treatment. The number of RNA assemblies and the fraction of cells with RNA assemblies are more than DAPI assemblies. Through microscopy images, it is evident that some DAPI assemblies undergo co-localization with RNA assemblies. Upon quantification we observe that around ~64% of the cells undergo co-localization and around ~60% of assemblies are seen to co-localize. *n=97 mock cells and n=111 treated cells*.

*Statistical test: Student t-test, ***p<0.0001, **p<0.05, non-significant (n.s.). Scalebar: 20µm.*

We speculated that the shRNA, albeit a scrambled control, could act as a pathogenic dsRNA for the cells, so we went ahead with a seemingly non-toxic plasmid that overexpresses H2B histone protein and possesses an mCherry tag.

We transfected 1µg of the plasmid and also co-transfected this plasmid with other kinds of nucleic acids like pENTR, a noncoding plasmid, and Poly I:C, synthetic dsRNA. These assemblies were observed in every transfection treatment (Figure 9(A)), and the morphology of these assemblies did not change. Upon quantifying the RNA intensity of the cytoplasm, we observed that there is ~8.4% reduction (significant) in treated cells (Figure 9(B)) as compared to mock-transfected cells. We also observed that in the nucleoplasm of the cells treated with 2µg DNA, the RNA intensity was reduced by ~10.6%. However, the reduction was not significant in other treatments. No significant difference was observed in the intensity of the nucleolus.

The number of these assemblies was measured and plotted (Figure 9(C)). We observed that the cells treated with a higher dose of plasmid vectors (2µg DNA) due to co-transfection showed ~45% more assemblies per cell than the cells treated with 1µg DNA. As compared to the cells treated with 1µg DNA+1µg RNA (Hybrid), 2µg DNA-treated cells had ~25% more assemblies. The cells possessing these assemblies were ~40% more in the 2 µg DNA treatment category than 1µg DNA treated cells and ~6.5% more as compared 1µg DNA+1µg RNA treated cells. Consequently, the co-localizing assemblies in the 2 µg DNA treated cells were also higher by ~43% as compared to the cells treated with 1 µg DNA and ~33% higher as compared to the cells treated with 1µg DNA+1µg RNA.

From these observations, we can conclude that the number of assemblies depends upon the dosage and the type of the nucleic acids used. All types of plasmid vectors lead to the formation of these nucleic acid assemblies. However, their number varies as per the treatment and dosage. In this case, the number of assemblies observed in the cells treated with 2 µg DNA> 1µg DNA+1µg RNA> 1 µg DNA (Figure 9).

(A)

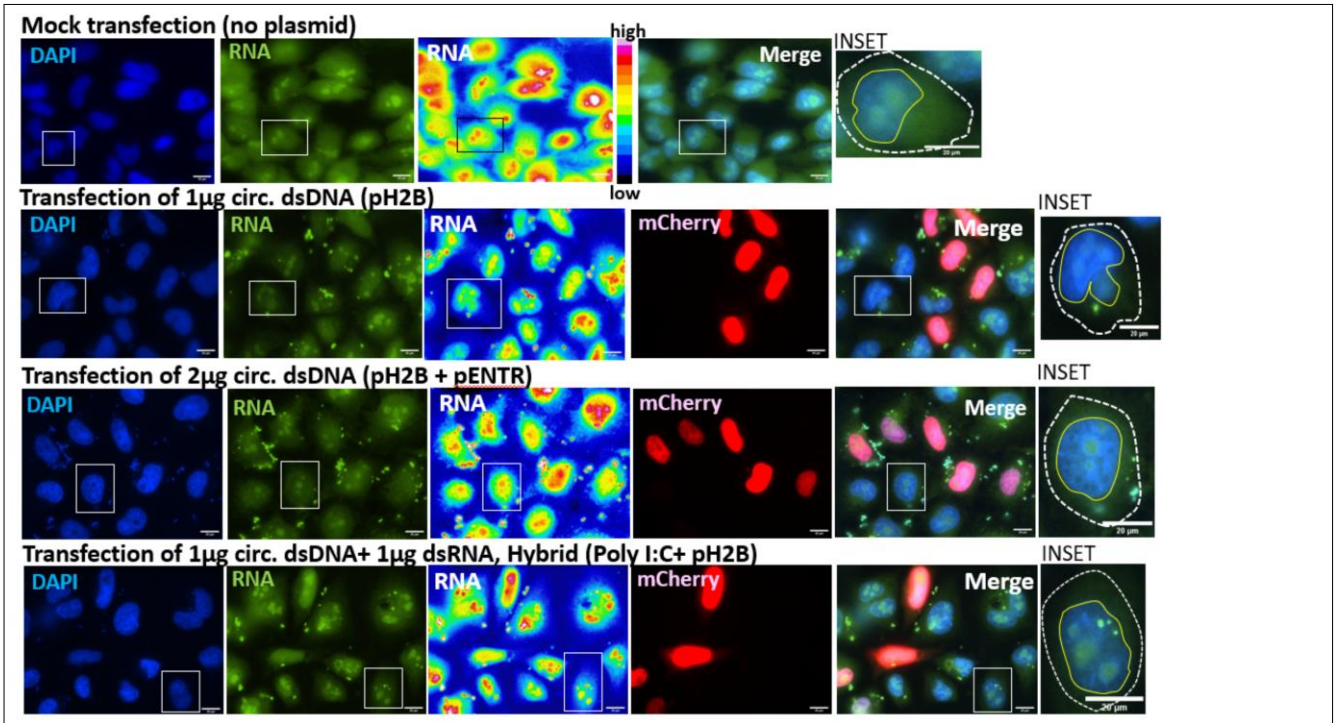
Mock transfection (no plasmid)
DAPI
RNA
RNA
high
low
Merge
INSET
Transfection of 1µg circ. dsDNA (pH2B)
mCherry
Transfection of 2µg circ. dsDNA (pH2B + pENTR)
Transfection of 1µg circ. dsDNA+ 1µg dsRNA, Hybrid (Poly I:C+ pH2B)

(B)

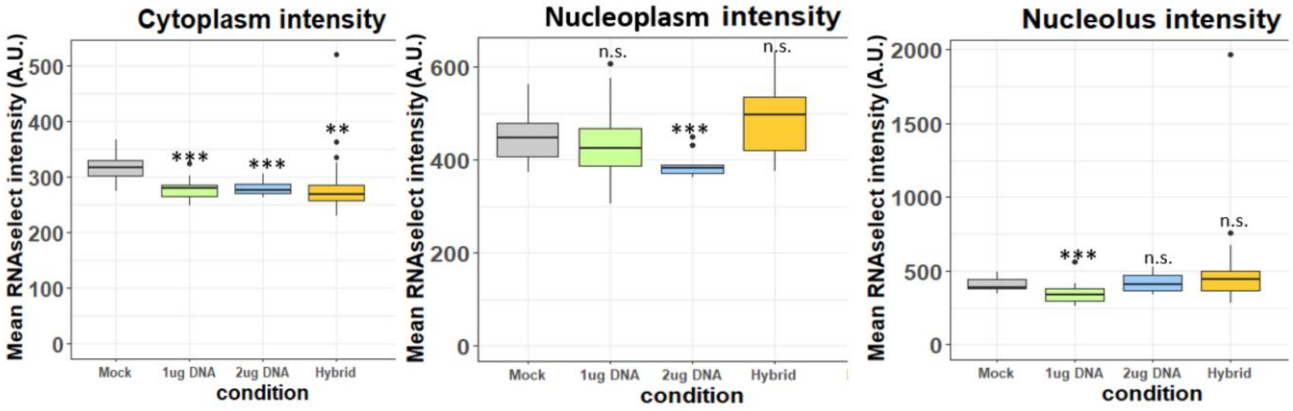
Cytoplasm intensity
Nucleoplasm intensity
Nucleolus intensity
Mean RNAselect intensity (A.U.)
condition
Mock
1ug DNA
2ug DNA
Hybrid
n.s.
***
**

(C)

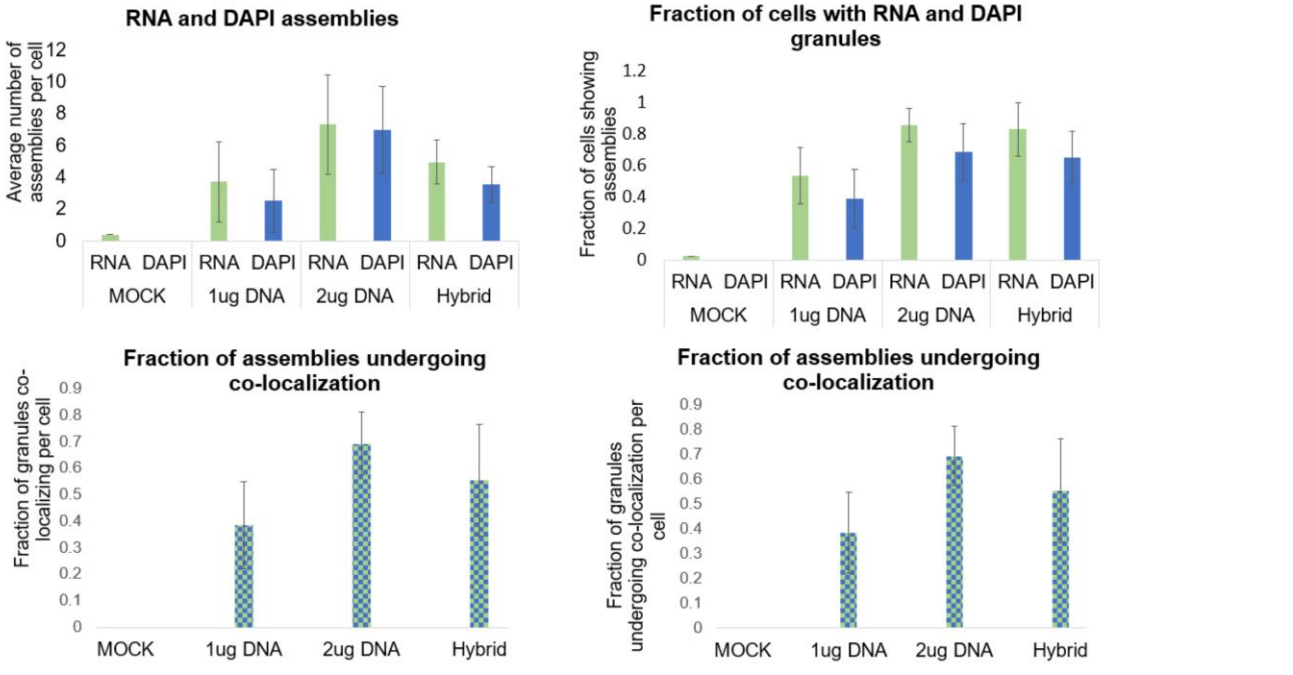
RNA and DAPI assemblies
Average number of assemblies per cell
Fraction of cells with RNA and DAPI granules
Fraction of cells showing assemblies
RNA DAPI
MOCK
1ug DNA
2ug DNA
Hybrid
Fraction of assemblies undergoing co-localization
Fraction of granules co-localizing per cell
Fraction of granules undergoing co-localization per cell

Figure 9: Transfection with different nucleic acids to check the presence of the assemblies
A) The cells were co-transfected with a mCherry-tagged plasmid. The images show the assemblies in all conditions and combinations. The cells treated with 2µg DNA show the greatest number of these assemblies B) Quantification of the RNA intensity levels in cytoplasm, nucleoplasm, and nucleolus. ~10% decrease (significant) in the RNA intensity of the cytoplasm of treated cells is observed as compared to the treated cells. The reduction is more prominent in cells treated with 2µg DNA. A significant reduction in the nucleoplasm of the 2µg DNA treated cells is also observed (~35%). Treatments include 1µg DNA, 2µg DNA, and 1µg DNA +1µg RNA respectively, *n=82 mock cells, n=20 1µg DNA treated cells, n=12 cells treated with 2µg DNA, and n=30 cells treated with 1µg DNA+1µg dsRNA.* C) Upon plotting the number of assemblies, we observe that they vary across treatments. The cells treated with 2µg DNA depict the highest number of assemblies, followed by 1µg DNA +1µg RNA treated cells, further followed by 1µg DNA treated cells. Order: 2µg DNA>1µg DNA +1µg RNA>1µg DNA. *n= 135 2µg DNA treated cells, n =135 1µg DNA+1µg RNA treated cells, n= 230 1µg DNA treated cells and n=104 mock-treated cells*

*Statistical test: Student t-test, ***p<0.0001, **p<0.05, non-significant (n.s.). Scalebar: 20µm*

3.3.2 Characterization of the observed assemblies

Next, we wanted to characterize these assemblies. We were unsure about the nature of these bodies so we speculated that these could be formed due to transfection, acting as a stress inducer. So, we checked if these assemblies co-localize with GTPase-activating protein-binding protein 1 (G3BP1), an RNA-binding protein found in stress granules. Stress granules are formed by mRNAs and ribonucleoproteins (RNPs) via the process of liquid-liquid phase separation when translation is inhibited. We transfected the cells and stained them with RNA and G3BP1. The nucleic acid assemblies were observed when the cells were transfected with the plasmid vector, and not all assemblies co-localized with G3BP1 (figure 10). We did not observe the assemblies when the cells were transfected with synthetic dsRNA, Poly IC. However, we observed some G3BP1 foci in Poly IC-treated cells. These foci were smaller and morphologically different from the nucleic acid assemblies, but they co-localized with equivalent RNA foci.

From these observations, we can conclude that treatment with Poly IC or synthetic dsRNA does not lead to the formation of nucleic acid assemblies. The plasmid vectors or circular dsDNA give rise to the formation of these assemblies. Complete co-localization of these assemblies with G3BP1 was not observed when the cells were treated with a plasmid vector. Additionally, in Poly IC treated cells, G3BP1 and RNA foci were observed. These foci were different from the assemblies.

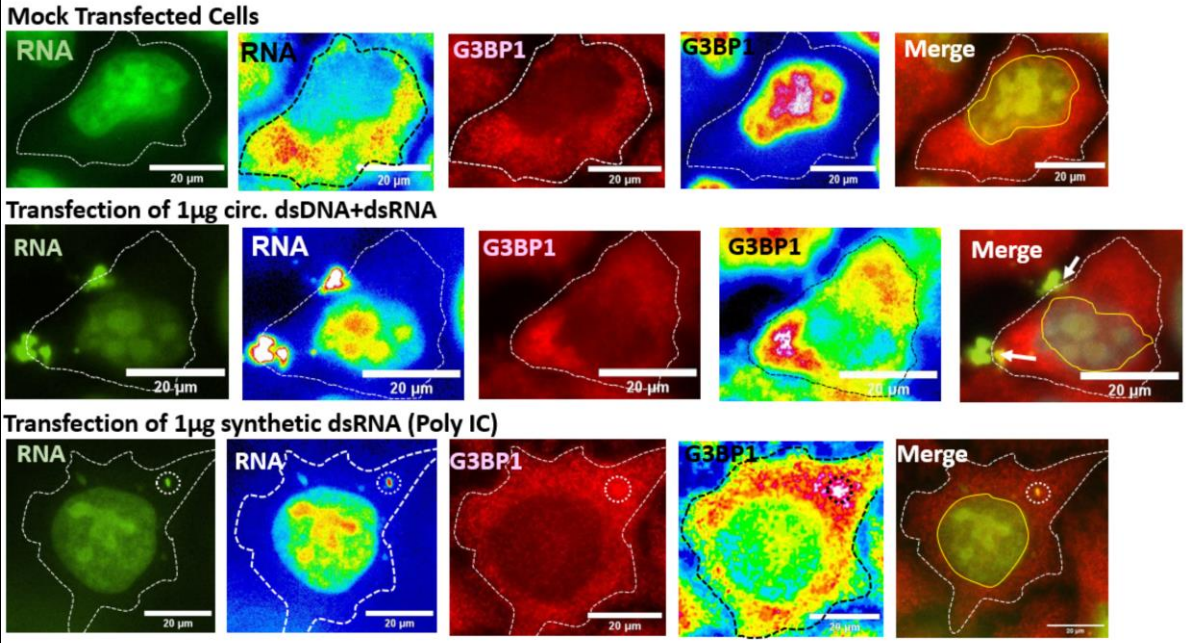

Figure 10: Checking co-localization of the nucleic acid assemblies with SGs. The cells were transfected with 1µg plasmid DNA encoding for a control shRNA and with 1µg Poly IC (synthetic dsRNA). The plasmid-treated cells showed the presence of observed nucleic acid assemblies. The nucleic acid assemblies did not completely co-localize with G3BP1. However, the Poly IC-treated cells did not show these assemblies. Instead, we observed smaller G3BP1 foci inside the cytoplasm that co-localized with RNA. The LUT image of G3BP1 verifies this observation- small and granular high-intensity foci are observed in Poly IC-treated cells. These foci are demarcated by white dotted circles.

Scalebar: 20 µm

From the microscopy images, it was observed that the majority of the assemblies formed are spherical. The phase condensates formed by liquid-liquid phase separation are often irregular in morphology and dynamic. Therefore, we wondered if a lipid membrane encloses these assemblies. We performed a co-localization assay with WGA (Wheat Germ Agglutinin) to check if that is the case. WGA binds to the glycoproteins of the lipid bilayer membrane.

The cells were transfected with 1 µg plasmid DNA, and it was observed that there is a complete co-localization of the nucleic acid assemblies with WGA (figure 11(A)). From the microscopy images, it was observed that these assemblies are mostly found right at the cell boundary or outside the cells. We also performed a conditioned media experiment where the supernatant of the treated cells was transferred to the untreated cells to check if these assemblies were in the supernatant. No assemblies were observed in cells treated with conditioned media.

Quantification of the RNA intensities showed a significant increase in intensity in the cytoplasm and nucleolus of the transfected cells (figure 11(B)), which is contradictory to what was observed in our earlier experiments. The increase in intensity in the cytoplasm and nucleolus of treated cells as compared to mock-transfected cells was ~11% and ~26%, respectively. However, a significant reduction in the RNA intensity of the cytoplasm, nucleolus, and nucleoplasm of the cells treated with conditioned media was observed. The reduction was ~15%, ~11%, and ~37%, respectively.

The number of RNA and DNA assemblies was measured and plotted (figure 11(C)). No assemblies were observed in the cells treated with conditioned media. The average number of RNA assemblies and DNA assemblies was ~3, and ~60% of the treated cells had these assemblies. ~70% of the RNA assemblies co-localized with DNA assemblies, and ~55% of the cells had assemblies that underwent co-localization.

From this experiment, we can conclude that the DNA and the RNA in these assemblies are enclosed within the membrane. An increase in RNA intensity was observed in the treated cells. No assemblies and a decrease in RNA intensity were observed in the cells treated with conditioned media.

(A)

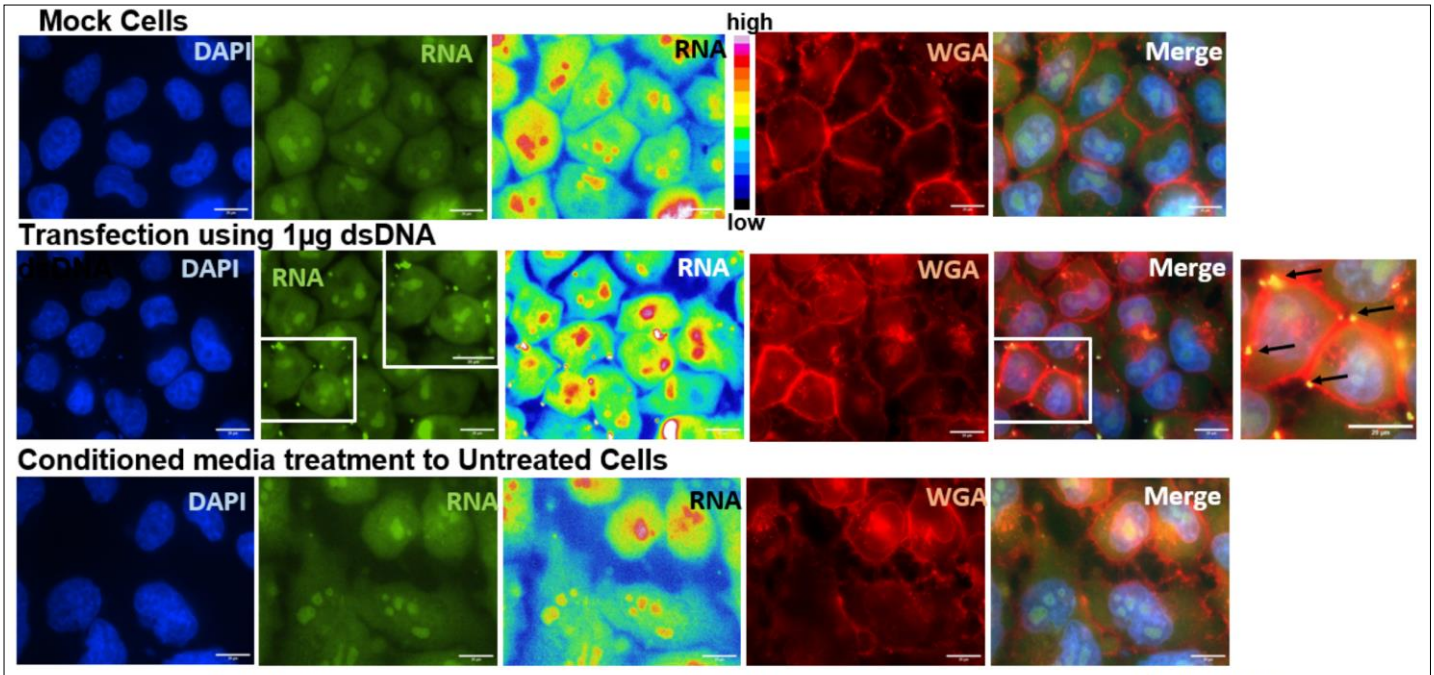
Mock Cells
DAPI
RNA
RNA
high
low
WGA
Merge
Transfection using 1µg dsDNA
DAPI
RNA
RNA
WGA
Merge
Conditioned media treatment to Untreated Cells
DAPI
RNA
RNA
WGA
Merge

(B)

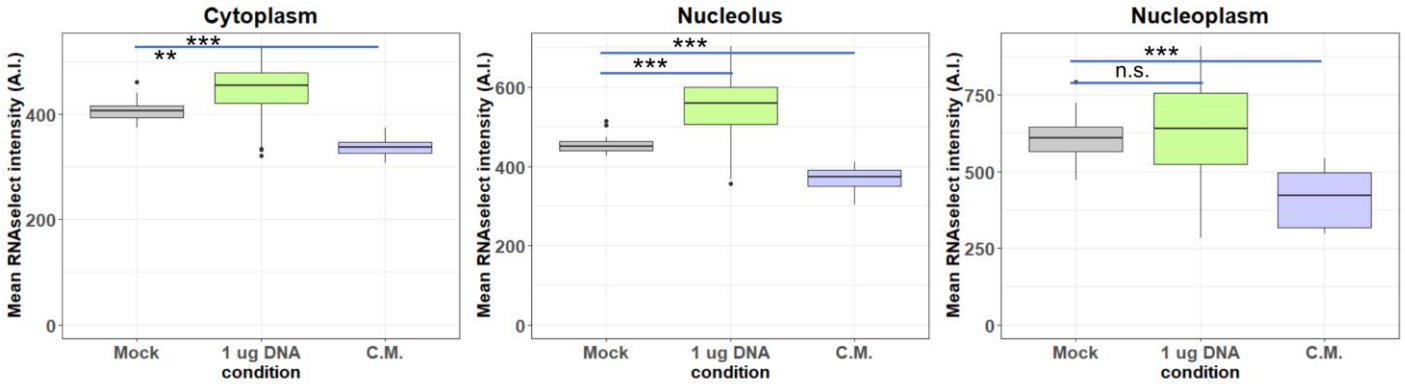
Cytoplasm
Nucleolus
Nucleoplasm
Mean RNAselect intensity (A.I.)
***
**
n.s.
Mock
1 ug DNA
C.M.
condition

(C)

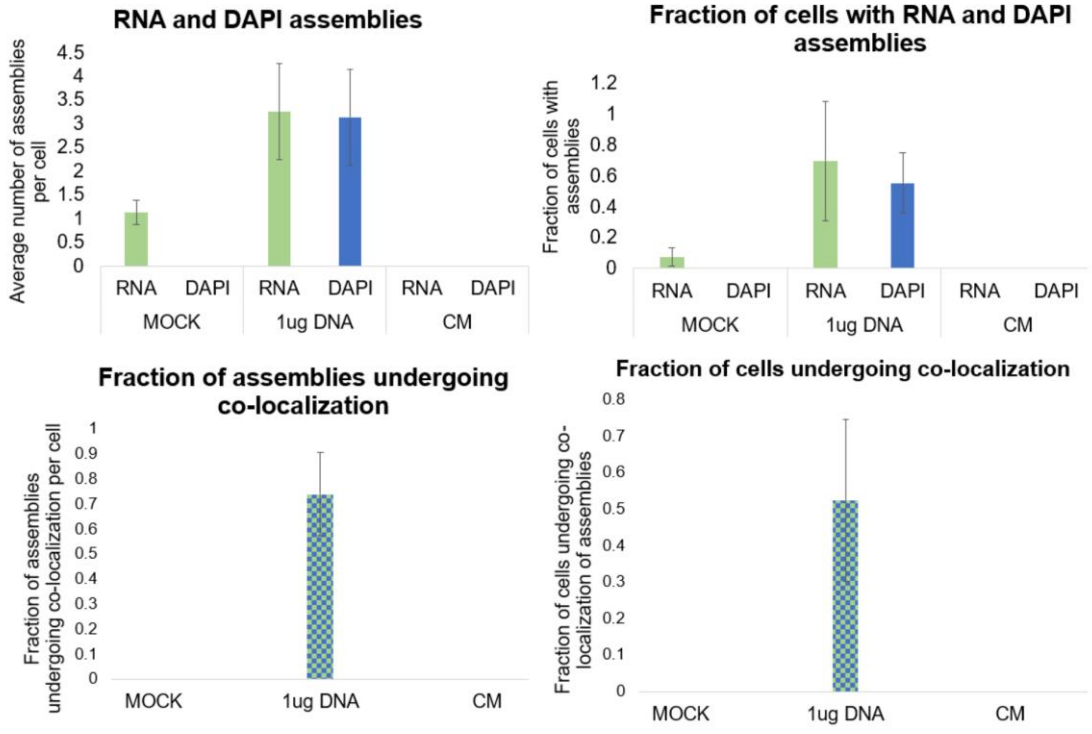
RNA and DAPI assemblies
Average number of assemblies per cell
Fraction of cells with RNA and DAPI assemblies
Fraction of cells with assemblies
RNA
DAPI
MOCK
1ug DNA
CM
Fraction of assemblies undergoing co-localization
Fraction of assemblies undergoing co-localization per cell
Fraction of cells undergoing co-localization
Fraction of cells undergoing co-localization of assemblies

Figure 11: Checking co-localization of nucleic-acid assemblies with WGA. (A) The cells were treated with 1 µg plasmid DNA and with conditioned media. The assemblies were observed in plasmid-treated cells but not in the cells treated with conditioned media. Black arrows show the assemblies co-localizing with WGA. (B) An increase in the RNA intensity was observed in the cytoplasm and nucleolus of treated cells. The increase in intensity in the nucleoplasm of the treated cells was not significant. A significant decrease in intensity in the cytoplasm, nucleolus, and nucleoplasm of cells treated with conditioned media was observed. (C) the average number of RNA and DNA assemblies in the treated cells were comparable. ~70% of the assemblies co-localized per cell, and the cells possessing co-localized assemblies were ~55%.

*Statistical test: Student t-test, ***p<0.0001, **p<0.05, non-significant (n.s.). Scalebar: 20µm.*

CONCLUSIONS

In summary, we can conclude (section 3.1) that the introduction of nucleic acids leads to the activation of type-I IFN response, thereby upregulating cytokines like IFNβ. The introduction of plasmid vectors, irrespective of their sequences, elicits a similar response, and Poly IC, a synthetic dsRNA, shows the highest IFNβ expression levels. It can be concluded that the cells activate an antiviral-like pathway upon sensing foreign nucleic acids and lead to the upregulation of RNase L expression levels. The increase in RNase L levels was similar across plasmid vectors and Poly IC. We speculated that increase in RNase L levels will lead to a decrease in RNA level. However, we did not see a clear degradation of RNA upon running the RNA samples on the gel. However, in section 3.3, we observed reduced total RNA levels in the treated cells. We also observed nucleic-acid assemblies enclosed by the membrane. In a majority of the experiments, ≥50% of these assemblies contained both DNA and RNA. The reduction in RNA levels in the cytoplasm (Figures 7,8, and 9) was consistent, but it seemed to vary in nucleolus and nucleoplasm (Figures 7 and 9). When the cells were stained for membrane (using WGA) and RNA (using RNAselect dye) together, an opposite trend was observed (figure 11). The treated cells showed enhanced RNA levels in the cytoplasm and nucleolus. However, the cells treated with conditioned media showed a reduction in the RNA levels in the cytoplasm, nucleoplasm, and nucleolus. The nucleic acid assemblies are observed only when the cells are treated with plasmid vectors. They are not observed when they are treated with Poly IC, a synthetic dsRNA (figure 10). Poly IC-treated cells show foci different from the observed assemblies. These foci are fewer in number and do not contain DNA. They co-localize with a stress granule protein, G3BP1. G3BP1 does not entirely co-localize with nucleic-acid assemblies.

Chapter 4 Discussion

Transfection of nucleic acids is a widely used strategy often employed to investigate gene expression. However, the process of introduction of non-self nucleic acids itself can lead to an alteration of nucleic acid metabolism by activating an antiviral-like pathway and inducing type-I IFN response as a consequence. The activation of the antiviral pathway increases the expression of nucleases to combat the pathogen posing a danger. A very crucial ribonuclease that is upregulated and activated upon pathogenic invasion is RNase L.

A synthetic dsRNA, Poly IC, acts as a mimic of the viral genome. It has been reported that Poly IC can induce type-I IFN response and enhance the expression of the IFNβ gene via the 2'-5'-oligoadenylate synthetase/RNase L (2-5A OAS-RNaseL) antiviral pathway (Banerjee *et al.*, 2014). However, we observed that transfecting plasmid vectors can also lead to an upregulation of inflammatory genes and RNase L levels. We observed enhanced IFNβ levels (Figure 4) and an increase in RNase L gene levels (Figure 5) upon transfecting with plasmid vectors encoding for control shRNA and mCherry protein. We speculate that the introduction of DNA vector is leading to the enhanced expression of RNase L and type-I IFN response by the cGAS-STING pathway (Fu *et al.*, 2020).

The activation of an antiviral-like pathway and upregulation of nucleases alters nucleic acid metabolism and changes the localization of nucleic acids. Studies have reported an altered localization and sequestration of the nucleic acids into membrane-less condensates (Maharana *et al.*, 2018; Zhou *et al.*, 2021; Xiao *et al.*, 2022). However, the assemblies we observed upon transfecting the cells with plasmid vectors, co-localized with a membrane dye, WGA (Figure 11(A)). The observed assemblies consisted of faint DAPI signals and were found to be rich in RNA. Moreover, the number of these assemblies increased when the cells were co-transfected, making the total concentration to 2µg DNA (Figure 9).

The characteristics of these assemblies and the co-localization data with WGA suggest that these assemblies have plasmid DNA and are surrounded by RNA. The majority of the nucleic acid assemblies were found outside the cells, near the

membrane. Therefore, there could be a chance that these assemblies are being translocated via the Golgi-trafficking pathway as observed in the cGAS-STING pathway upon activation of STING (Ishikawa *et al.*, 2009). WGA stains for the vesicles involved in the Golgi-trafficking pathway (Allen *et al.*, 1989). Moreover, the packaged RNA in the vesicles being exocytosed explain the reduction in the RNA intensities observed when the cells are treated with plasmid vectors (Figure 7, 8, and 9). We also observed a couple of contradictory observations. First, when the cells were treated and stained with WGA- the RNA intensity in the treated cells was higher (Figure 11). We speculate that this could be due to WGA interfering with the RNAselect dye. Second, the RNA gel did not show clear degradation (Figure 6). This could be because quantification through the gel is a crude way. Going forward, a more sensitive technique like metabolic labeling could be used to confirm if RNA degradation or a decrease in transcription is the cause for reduced RNA levels observed via quantification of microscopy images.

The introduction of synthetic dsRNA, Poly IC, did not lead to the formation of these assemblies (Figure 10). However, it led to the formation of foci containing RNA and G3BP1. Recently, a study reported the formation of such foci in Poly IC transfected cells formed due to the activation of RNase L (Burke *et al.*, 2020). These foci were called RNase L-dependent bodies (RLBs). We believe that the foci we observed in Poly IC-treated cells are similar to RLBs.

In summary, our results show that transfection or introduction of non-self nucleic acids leads to the upregulation of an inflammatory response pathway and alters nucleic acid metabolism in cells by upregulating RNases. A change in RNA localization is depicted by the formation of RNA-rich assemblies. These assemblies are enclosed by a lipid bilayer membrane and are formed when a plasmid vector is transfected.

HYPOTHETICAL MODEL:

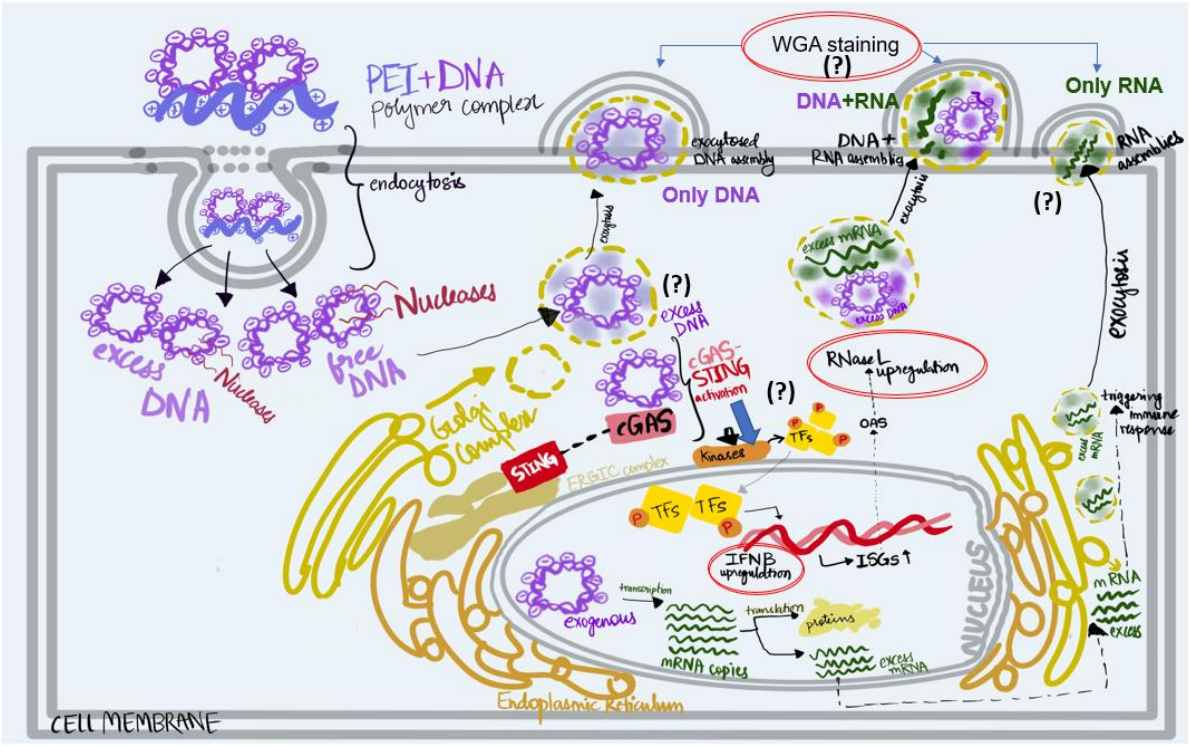

Figure 12: A hypothetical model based on the results observed in the study. The figure depicts a transfected cell representing our interpretation of the results and a plausible model encompassing the processes that could be taking place upon treatment with circular dsDNA.

Red ovals: shown in this study
Question marks: Limitations of the study

.

First, the PEI forms a complex with DNA which is taken up by endocytosis. The free DNA is then released into the cytoplasm. Most of the free DNA is cleaved by the nucleases, however, some free DNA copies trigger cGAS-STING signalling based immune response pathway. The cGAS senses dsDNA in the cytoplasm and with STING, which sits in the intermediate complex of ER and Golgi (ERGIC complex), recruits kinases and phosphorylates transcription factors (TFs). The phosphorylated TFs translocate to the nucleus and upregulates IFN-stimulated genes or ISGs. One of the important ISG is IFNβ which was shown to be upregulated in this study. Another important ISG is OAS (oligoadenylate synthetase) which gets activated by the IFNs and also by the presence of dsRNA in the cytoplasm. The OAS upregulation and activation would lead to the upregulation and activation of RNase L, an antiviral Ribonuclease. The upregulation of RNase L was shown in this study. However, the activation of cGAS-STING pathway was not shown.

We believe that other free DNA copies would lead to their exocytosis via Golgi vesicles through lysosomal pathways and this is speculation made based on our WGA staining results as WGA stains for golgi-associated vesicles. Some dsDNA copies enter nucleus and lead to the production of excess mRNAs. Some mRNA copies are translated into the proteins; however, the excess free mRNAs are transported in the cytoplasm leading to their exocytosis via Golgi vesicles. This corroborates our results that we observe only DNA assemblies and only RNA assemblies. The co-localizing assemblies are formed when the free excess mRNA copies and the free DNA copies are encapsulated in the same golgi-formed vesicles and exocytosed. This study did not characterize these assemblies hence, we cannot discern their composition as of yet. These speculations are based on WGA staining but the presence of the membranes need to be confirmed via other techniques.

Chapter 5 Future Directions

As we advance with the study of nucleic acid metabolism and its role in causing an inflammatory response, there are several directions that can be pursued to gain a deeper understanding of the mechanistic pathway involved. One approach would be to investigate the expression and activation of various other inflammatory cytokines and IFNs like IL-1β, IL-8, TNFα, etc. using qRT-PCR and Western Blotting. Additionally, the activation of RNase L and the genes and kinases like TBK1, involved in the cGAS-STING pathway can be targeted to understand their role in the pathway.

To better characterize the observed nucleic acid assemblies, FRAP (Fluorescence recovery after photobleaching) can be performed to examine their dynamicity, and metabolic labeling using ethynyl-uridine can be used to investigate total RNA levels in a more sensitive manner. Co-staining with endosome markers like Rab5 and Rab7 would confirm the translocation of these assemblies via endosomes and lysosomes. Live-cell imaging using a tagged probe after transfection would also be useful for monitoring the movement of these assemblies within the cells.

It would be beneficial to use a point scanning, confocal microscope instead of a wide-field microscope to visualize images stained with WGA. This would allow for z-stacks of the images, providing information about the location of the assemblies within the cells.

To investigate the occurrence of these assemblies, better control experiments can be performed using labeled ssDNA, dsDNA, ssRNA, and dsRNA. By taking these future directions, we can gain a more comprehensive understanding of the mechanism underlying the alteration of nucleic acid metabolism and its role in causing an inflammatory response upon the transfection of nucleic acids.

Pursuing the aforementioned directions, more detailed and comprehensive elucidation of the underlying mechanism of nucleic acid sensing pathways and the associated innate immune response can be achieved.

References

- Allen, RD, Schroeder, CC, and Fok, AK (1989). Intracellular binding of wheat germ agglutinin by Golgi complexes, phagosomes, and lysosomes of Paramecium multimicronucleatum. J Histochem Cytochem 37, 195–202.
- Banani, SF, Lee, HO, Hyman, AA, and Rosen, MK (2017). Biomolecular condensates: organizers of cellular biochemistry. Nat Rev Mol Cell Biol 18, 285–298.
- Banerjee, S, Chakrabarti, A, Jha, BK, Weiss, SR, and Silverman, RH (2014). Cell-Type-Specific Effects of RNase L on Viral Induction of Beta Interferon. MBio 5, e00856-14.
- Bisbal, C, and Silverman, RH (2007). Diverse functions of RNase L and implications in pathology. Biochimie 89, 789–798.
- Bridge, AJ, Pebernard, S, Ducraux, A, Nicoulaz, A-L, and Iggo, R (2003). Induction of an interferon response by RNAi vectors in mammalian cells. Nat Genet 34, 263–264.
- Burke, JM, Lester, ET, Tauber, D, and Parker, R (2020). RNase L promotes the formation of unique ribonucleoprotein granules distinct from stress granules. J Biol Chem 295, 1426–1438.
- Chakrabarti, A, Ghosh, PK, Banerjee, S, Gaughan, C, and Silverman, RH (2012). RNase L Triggers Autophagy in Response to Viral Infections. J Virol 86, 11311–11321.
- Chien, Y et al. (2006). RalB GTPase-Mediated Activation of the IκB Family Kinase TBK1 Couples Innate Immune Signaling to Tumor Cell Survival. Cell 127, 157–170.
- Chow, KT, Gale, M, and Loo, Y-M (2018). RIG-I and Other RNA Sensors in Antiviral Immunity. Annu Rev Immunol 36, 667–694.
- Crow, YJ, and Stetson, DB (2022). The type I interferonopathies: 10 years on. Nat Rev Immunol 22, 471–483.
- Du, M, and Chen, ZJ (2018). DNA-induced liquid phase condensation of cGAS activates innate immune signaling. Science 361, 704–709.
- Fu, Y et al. (2020). Inhibition of cGAS-Mediated Interferon Response Facilitates Transgene Expression. IScience 23, 101026.
- Girardin, SE et al. (2003a). Nod1 Detects a Unique Muropeptide from Gram-Negative Bacterial Peptidoglycan. Science 300, 1584–1587.
- Girardin, SE, Boneca, IG, Viala, J, Chamaillard, M, Labigne, A, Thomas, G, Philpott, DJ, and Sansonetti, PJ (2003b). Nod2 Is a General Sensor of Peptidoglycan through Muramyl Dipeptide (MDP) Detection. J Biol Chem 278, 8869–8872.
- Goubau, D et al. (2014). Antiviral immunity via RIG-I-mediated recognition of RNA bearing 5′-diphosphates. Nature 514, 372–375.
- Greulich, W, Wagner, M, Gaidt, MM, Stafford, C, Cheng, Y, Linder, A, Carell, T, and Hornung, V (2019). TLR8 Is a Sensor of RNase T2 Degradation Products. Cell 179, 1264-1275.e13.
- Guo, W, and Novick, P (2004). The exocyst meets the translocon: a regulatory circuit for secretion and protein synthesis? Trends Cell Biol 14, 61–63.
- Hemmi, H et al. (2000). A Toll-like receptor recognizes bacterial DNA. Nature 408, 740–745.

- Honda, K, Yanai, H, Takaoka, A, and Taniguchi, T (2005). Regulation of the type I IFN induction: a current view. Int Immunol 17, 1367–1378.
- Hornung, V, Ablasser, A, Charrel-Dennis, M, Bauernfeind, F, Horvath, G, Caffrey, DanielR, Latz, E, and Fitzgerald, KA (2009). AIM2 recognizes cytosolic dsDNA and forms a caspase-1-activating inflammasome with ASC. Nature 458, 514–518.
- Huang, H et al. (2014). Dimeric Structure of Pseudokinase RNase L Bound to 2-5A Reveals a Basis for Interferon-Induced Antiviral Activity. Mol Cell 53, 221–234.
- Husain, B, Mukerji, I, and Cole, JL (2012). Analysis of High-Affinity Binding of Protein Kinase R to Double-Stranded RNA. Biochemistry 51, 8764–8770.
- Ishikawa, H, and Barber, GN (2008). STING is an endoplasmic reticulum adaptor that facilitates innate immune signalling. Nature 455, 674–678.
- Ishikawa, H, Ma, Z, and Barber, GN (2009). STING regulates intracellular DNA-mediated, type I interferon-dependent innate immunity. Nature 461, 788–792.
- Janeway, CA (1989). Approaching the Asymptote? Evolution and Revolution in Immunology. Cold Spring Harb Symp Quant Biol 54, 1–13.
- Jha, BK, Polyakova, I, Kessler, P, Dong, B, Dickerman, B, Sen, GC, and Silverman, RH (2011). Inhibition of RNase L and RNA-dependent Protein Kinase (PKR) by Sunitinib Impairs Antiviral Innate Immunity. J Biol Chem 286, 26319–26326.
- Kang, D, Gopalkrishnan, RV, Wu, Q, Jankowsky, E, Pyle, AM, and Fisher, PB (2002). *mda-5*: An interferon-inducible putative RNA helicase with double-stranded RNA-dependent ATPase activity and melanoma growth-suppressive properties. Proc Natl Acad Sci 99, 637–642.
- Kawai, T Toll-like receptor signaling pathways. Front Immunol.
- Kawai, T, and Akira, S (2010). The role of pattern-recognition receptors in innate immunity: update on Toll-like receptors. Nat Immunol 11, 373–384.
- Kawasaki, T, Kawai, T, and Akira, S (2011). Recognition of nucleic acids by pattern-recognition receptors and its relevance in autoimmunity: Nucleic acid recognition and autoimmunity. Immunol Rev 243, 61–73.
- Keating, SE, Baran, M, and Bowie, AG (2011). Cytosolic DNA sensors regulating type I interferon induction. Trends Immunol 32, 574–581.
- Lee, BL, and Barton, GM (2014). Trafficking of endosomal Toll-like receptors. Trends Cell Biol 24, 360–369.
- Li, X, Shu, C, Yi, G, Chaton, CT, Shelton, CL, Diao, J, Zuo, X, Kao, CC, Herr, AB, and Li, P (2013). Cyclic GMP-AMP Synthase Is Activated by Double-Stranded DNA-Induced Oligomerization. Immunity 39, 1019–1031.
- Li, Y, Banerjee, S, Wang, Y, Goldstein, SA, Dong, B, Gaughan, C, Silverman, RH, and Weiss, SR (2016). Activation of RNase L is dependent on OAS3 expression during infection with diverse human viruses. Proc Natl Acad Sci 113, 2241–2246.
- Maharana, S et al. (2018). RNA buffers the phase separation behavior of prion-like RNA binding proteins. Science 360, 918–921.
- Maharana, S et al. (2022). SAMHD1 controls innate immunity by regulating condensation of immunogenic self RNA. Mol Cell 82, 3712-3728.e10.

- Malathi, K, Dong, B, Gale, M, and Silverman, RH (2007). Small self-RNA generated by RNase L amplifies antiviral innate immunity. Nature 448, 816–819.
- Miyake, K, Shibata, T, Ohto, U, Shimizu, T, Saitoh, S-I, Fukui, R, and Murakami, Y (2018). Mechanisms controlling nucleic acid-sensing Toll-like receptors. Int Immunol 30, 43–51.
- Okude, H, Ori, D, and Kawai, T (2021). Signaling Through Nucleic Acid Sensors and Their Roles in Inflammatory Diseases. Front Immunol 11, 625833.
- Paget, M et al. (2021). Stress granules are shock absorbers that prevent excessive innate immune responses to dsRNA, Immunology.
- Pebernard, S, and Iggo, RD (2004). Determinants of interferon-stimulated gene induction by RNAi vectors. Differentiation 72, 103–111.
- Pelka, K, Shibata, T, Miyake, K, and Latz, E (2016). Nucleic acid-sensing TLRs and autoimmunity: novel insights from structural and cell biology. Immunol Rev 269, 60–75.
- Rock, FL, Hardiman, G, Timans, JC, Kastelein, RA, and Bazan, JF (1998). A family of human receptors structurally related to *Drosophila* Toll. Proc Natl Acad Sci 95, 588–593.
- Savva, YA, Rieder, LE, and Reenan, RA (2012). The ADAR protein family. Genome Biol 13, 252.
- Schlee, M, and Hartmann, G (2016). Discriminating self from non-self in nucleic acid sensing. Nat Rev Immunol 16, 566–580.
- Shu, C, Li, X, and Li, P (2014). The mechanism of double-stranded DNA sensing through the cGAS-STING pathway. Cytokine Growth Factor Rev 25, 641–648.
- Silva-Gomes, S, Decout, A, and Nigou, J (2014). Pathogen-Associated Molecular Patterns (PAMPs). In: Encyclopedia of Inflammatory Diseases, ed. M Parnham, Basel: Springer Basel, 1–16.
- Takeuchi, O, and Akira, S (2010). Pattern Recognition Receptors and Inflammation. Cell 140, 805–820.
- Webb, LG, and Fernandez-Sesma, A (2022). RNA viruses and the cGAS-STING pathway: reframing our understanding of innate immune sensing. Curr Opin Virol 53, 101206.
- Wu, J, Sun, L, Chen, X, Du, F, Shi, H, Chen, C, and Chen, ZJ (2013). Cyclic GMP-AMP Is an Endogenous Second Messenger in Innate Immune Signaling by Cytosolic DNA. Science 339, 826–830.
- Wu, L, Xu, Y, Zhao, H, and Li, Y (2020). RNase T2 in Inflammation and Cancer: Immunological and Biological Views. Front Immunol 11, 1554.
- Xiao, Q, McAtee, CK, and Su, X (2022). Phase separation in immune signalling. Nat Rev Immunol 22, 188–199.
- Yoneyama, M, Kikuchi, M, Natsukawa, T, Shinobu, N, Imaizumi, T, Miyagishi, M, Taira, K, Akira, S, and Fujita, T (2004). The RNA helicase RIG-I has an essential function in double-stranded RNA-induced innate antiviral responses. Nat Immunol 5, 730–737.
- Zhou, W, Mohr, L, Maciejowski, J, and Kranzusch, PJ (2021). cGAS phase separation inhibits TREX1-mediated DNA degradation and enhances cytosolic DNA sensing. Mol Cell 81, 739-755.e7.